Event-Triggered Fixed-Time Control for Steer-by-Wire Systems With Prespecified Tracking Performance

Bingxin Ma
Northeastern University
Gang Luo
Northeastern University
Yongfu Wang (dongdaneu@163.com)
Northeastern University

Research Article

Keywords: Steer-by-wire (SbW) system , Event-triggered communication , Fuzzy-based state observer , Fixed-time contron , Prespecified tracking performance

Posted Date: April 6th, 2021

DOI: https://doi.org/10.21203/rs.3.rs-370605/v1

Noname manuscript No.
(will be inserted by the editor)

Event-Triggered Fixed-Time Control for Steer-by-Wire Systems With Prespecified Tracking Performance

Bingxin Ma · Gang Luo · Yongfu Wang

Received: date / Accepted: date

Abstract This paper addresses the event-triggered output feedback control problem for (steer-by-wire) SbW systems with uncertain nonlinearity and time-varying disturbance. First, a new framework of event-triggered control systems is proposed to eliminate the jumping phenomenon of event-based control input, and the tradeoff between saving communication resources and attenuating jumping phenomenon can be removed. Then, the adaptive disturbance observer and fuzzy-based state observer are developed to estimate the external disturbance and unavailable state of augmented SbW systems, respectively. Third, an event-triggered fixed-time control is developed for SbW systems to achieve prespecified tracking accuracy while saving communication resources of the controller area network (CAN). Furthermore, theoretical analysis based on Lyapunov stability theory is provided to verify the tracking error of SbW systems can converge to the prespecified neighborhood of the origin in fixed time regardless of the initial tracking error. Finally, simulations and experiments are given to evaluate the effectiveness and superiority of the proposed methods.

Keywords Steer-by-wire (SbW) system · Event-triggered communication · Fuzzy-based state observer · Fixed-time contron · Prespecified tracking performance

Bingxin Ma
E-mail: bingxinma1710116@126.com
Gang Luo
E-mail: m15940256365@163.com

Yongfu Wang(✉)
E-mail: dongdaneu@163.com
School of Mechanical Engineering and Automation, Northeastern University, Shenyang, Liaoning 110819, China

1 Introduction

The steer-by-wire (SbW) system is one of the main subsystems of autonomous vehicles, realizing the steering control of front-wheels. Compared with the conventional steering system, SbW systems have two distinct characteristics: 1) the mechanical linkage between the steering wheel and front-wheels is no longer required; 2) the additional sensors, steering motor actuator, control unit, and controller area network (CAN) are necessary for SbW systems. Although the steering control of autonomous vehicles can be achieved through the SbW system, it is still a challenge to achieve accurate modeling and control of the SbW system with measurement and communication limitations [1–5].

Significant contributions have been made to the literature of SbW control systems; see, e.g., [6–15] and the references therein. Representatively, the model-based control method, such as proportional-integral-derivative control [6], proportional-derivative control with feedforward compensation [7], and model predictive control [8] are nvestigated for SbW systems. Considering the SbW system's parametric uncertainties and disturbances, the fairly accurate state model and robust sliding mode control are first reported in [9]. Then, the adaptive sliding mode control method of SbW systems is investigated in [10–13] without *a priori* bounds of uncertainties and disturbances. References [14, 15] address the active fault-tolerant control problem of SbW systems subject to modeling uncertainties and disturbances with *a priori* bounds. A detailed literature review of the SbW control system can be found in Tab.1. Although the methods mentioned above have obtained fruitful achievements in SbW control systems, there are still the following limitations: 1) multi-sensor measurement technology is required in the control application,

Table 1 A summary of SbW control systems

Rreference	Technique	Main limitations
Rreferences[6–8]	Model-based control method	1) Multi-sensor measurement technology is required in the control application, which increases the hardware complexity and cost of SbW systems, and 2) the uninterrupted transmission of the control input to the steering motor is required, which occupies unnecessary CAN communication resources.
Rreferences[9–13]	Sliding mode control for uncertain SbW systems with disturbance	
Rreferences[14, 15]	Model predictive control for SbW systems with actuator fault	

Table 2 A summary of state estimators

Rreference	Technique	Assumptions or limitations
Rreferences[16, 17]	Sliding mode differentiator	k-th derivative of signal with the known Lipschitz constant or bounded function.
Rreference [18]	Sliding mode differentiator for nonlinear mechanical systems	The input and output of controlled systems should be bounded.
Rreferences[19, 20]	Sliding-mode observer of uncertain Lagrangian systems	The bounds of uncertainties must be *a priori*.
Rreferences[21–23]	First-order low-pass	The derivative of signals must be bounded.
Rreferences[24, 25]	High-gain observer	The accurate model of nonlinear system are known.
Rreferences[26–31]	Approximator-based observer	The convergence of observation errors is asymptotic rather than fixed-time.

Table 3 A summary of event-triggered control systems

Rreference	Technique	Main limitations
Rreferences[32–34]	ISS-based event-triggered control for nonlinear systems	1) The jumping phenomenon of the control input caused by event-triggered communicatuion has not been considered in [27, 28, 31–38]; 2) it is difficult to solve the trade-off between saving communication resources and attenuating jumping phenomenon, and the jumping phenomenon still exists in [39, 40]; and 3) the transient and steady performance of control systems cannot be guaranteed at the same time.
Rreferences[35, 36]	Model-based event-triggered control for nonlinear systems	
Rreferences[27, 28, 31, 37, 38]	Adaptive Event-triggered control for uncertan nonlinear systems	
Rreferences[39, 40]	Jumping-attenuation event-triggered control	

which increases the hardware complexity and cost of SbW systems, and 2) the uninterrupted transmission of the control input to the steering motor is required, which will occupy unnecessary CAN communication resources. In practical applications, the vehicle-mounted CAN with limited communication channel bandwidth is usually shared by different nodes, so addressing the communication constraints is of great significance.

To reduce the use of sensors in control systems, significant contributions have been made to the literature of the state estimator. Representatively, the sliding mode differentiator is proposed in [16] for the signal with the k-th derivative having a known positive Lipschitz constant. Reference [17] develops a robust kth-order differentiation for signals with a given functional bound of the $(k+1)$-th derivative. Reference [18] proposes the sliding mode differentiator for nonlinear mechanical systems with bounded-input-bounded-state (BIBO) property. Reference [19, 20] proposes a global sliding mode observer for nonlinear mechanical systems subject to the Coriolis term and uncertainty with *a priori* bound. The first-order low-pass is considered the differentiator for signals with bounded derivatives[21–23], and the high-gain observer is developed for nonlinear systems with accurate model [24, 25]. Although the above state estimators are useful in some particular applications, they are challenging to achieve satisfactory estimation performance for SbW systems without BIBO property, bounded derivatives of state, accurate model, and *a priori* bounds of uncertainty/disturbance.

To this end, the approximator-based observer is proposed in [26–31], but the convergence of observation errors is asymptotic rather than lemma.fixed.time -time. For this reason, this paper proposes an adaptive state observer for an uncertain SbW system without the above assumptions and limitations shown in Tab.2.

In network control systems, the communication networks are usually shared by different system nodes, while the network resources including communication channel bandwidth and computation, abilities are limited. To reduce the unnecessary waste of communication resources, great efforts have been made to develop event-triggered control, in which information transmission occurs only when necessary, rather than continuously; see, e.g., [27, 28, 31–40] and the references therein. Specifically, with the assumption of the input-to-state stability (ISS), the event-triggered stabilization and tracking problem of nonlinear systems are addressed in [32–34], respectively. In [35, 36], the model-based event-triggered control method is proposed for network-based plants. Considering the model uncertainty of nonlinear systems, the event-triggered state and output feedback control are developed in [37, 38] and [27, 28, 31], respectively. It is worth mentioning that the control input is updated and transmitted only at event-triggered instants, so the jumping phenomenon of control input caused by communication is inevitable. Consequently, the large impulse will be applied to the system, especially in event-triggered control systems with relative threshold, which certainly affects the smoothness of actuator output and degrade the system performance[39, 40].

To this end, the switching triggered strategy, including fixed threshold strategy and relative threshold strategy, is proposed in [39, 40] to attenuate the jumping phenomenon of event-based control input. As shown in Fig.1(a), the core idea of the switching triggered strategy is that the fixed threshold strategy will be applied when the amplitude of control input is large, and the relative scheme will be applied when the amplitude of control input is small. Thereby, the event-triggered error has been constrained within the bounds of a constant, and the jumping phenomenon can be attenuated while saving communication resources as much as possible in this context. Unfortunately, it is difficult to solve the trade-off between saving communication resources and attenuating the jumping phenomenon, and the jumping phenomenon still exists in [39, 40]. This makes it difficult for the existing event-triggered control system to be applied to electromechanical systems with higher requirements for the smoothness of their actuators. Much imoportantly, the practical stability can be achieved asymptotically or within finite-time rather that fixed-time, which cannot guarantee the transient performance of closed-loop systems.

It is essential to save communication resources and reduce hardware costs from applying and developing network-controlled SbW systems. Simultaneously, to ensure vehicles' safety and comfort, it is necessary to achieve fixed-time prespecified tracking performance while guaranteeing the smoothness of the SbW system steering motor's output. As mentioned in Tab. 1 and Tab. 3, the existing SbW control systems and event-triggered control systems cannot meet these requirements and should be improved. For this reason, this paper proposes an even-triggered output feedback control method for SbW systems. The contributions of this paper are summarized in the following aspects:

(1) *From the perspective of even-triggered control system design*: A new framework of the event-triggered control system is proposed in this paper. 1) Combined with the event-triggered control systems in [27, 28, 31–38], as shown in Fig.1(b), the jumping phenomenon of control input can be eliminated, and 2) compared with the event-triggered control systems in [39, 40], the trade-off between saving communication resources and attenuating jumping phenomenon can be removed.

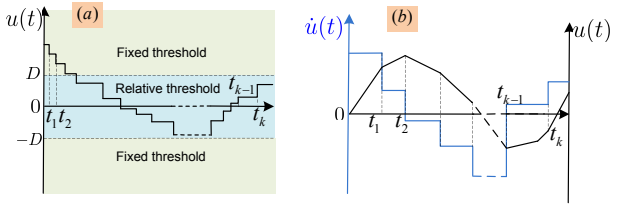

Fig. 1 Event-triggered control input. (a) Control input in [39, 40], (b) Control input in the designed event-triggered control system.

(2) *From the perspective of state observe design*: An adaptive state observer for an uncertain SbW system without the above assumptions and limitations shown in Tab. 2 is proposed in this paper. 1) Compared with recent researches on state observer [16–19, 41, 42], there is no need for additional assumptions, such that bounded-state property, bounded higher-order derivatives of output, and *a priori* known nonlinearities, and 2) compared with recent researches on FLS/NN-based state observer [27, 28, 30, 43, 44], the convergence speed of the observation error can be improved in this paper, i.e., the observation error can converge to the adjustable neighborhood of the origin in finite-time instead of asymptotically converging to the small neighborhood of the origin.

(3) *From the perspective of control method design*: An observer-based event-triggered fixed-time control is proposed for uncertain SbW systems regardless of the initial tracking error. 1) Compared with SbW control systems [9–15], the unnecessary sensor can be removed and CAN communication resources can be saved, 2) compared with event-triggered output feedback control [28, 31, 40], the prespecified tracking performance can be achieved within fixed time, so both the transient and steady performance of closed-loop systems can be guaranteed, and 3) compared with [27], the bounds of the initial state of the controlled system is no longer required.

The rest of the paper is organized as follows. In Section II, problem formulation and preliminaries are given. The fuzzy-based state-observer and event-triggered fixed time control is presented in Section III. The simulation and experiment are given in Section IV. Section V is the concluding remarks.

Notations: For a matrix A, $\|A\|$ denotes the Euclidean norm of A, and $\lambda_{\max(\min)}(A)$ denotes its maximum (minimum) eigenvalue. $\lfloor x \rceil^{\varrho} = |x|^{\varrho}\text{sign}(x)$ with $\varrho \geq 0$.

2 Problem Formulation and Preliminaries

Fig. 2 shows a schematic diagram of the SbW system for automatic vehicles. To describe the dynamics model clearly, Tab. 4 is given to clarify each of the components in Fig. 2.

2.1 Problem formulation

According to the researches [7, 9, 10, 45], the dynamics model of the steering motor can be established as

$$\mathcal{J}_m\ddot{\theta}_m + \mathcal{B}_m\dot{\theta}_m + \tau_{12} = \tau_m + \tau_d. \tag{1}$$

The rotation of the front-wheels around their vertical axes can be modeled as

$$\mathcal{J}_f\ddot{\theta}_f + \mathcal{H}_f(\theta_f, \dot{\theta}_f) = \tau_s \tag{2}$$

where $\mathcal{H}_f(\theta_f, \dot{\theta}_f) = \tau_e + \tau_f$ denotes the uncertain nonlinearity. The transmission ratio between the steering motor and front-wheels is

$$\frac{\theta_f}{\theta_m} = \frac{\dot{\theta}_f}{\dot{\theta}_m} = \frac{\ddot{\theta}_f}{\ddot{\theta}_m} = \frac{\tau_{12}}{\tau_s} = \frac{1}{\mu} \tag{3}$$

which together with (1)-(2) gets

$$\mathcal{J}_e\ddot{\theta}_f + \mu^2\mathcal{B}_m\dot{\theta}_f + \mathcal{H}_f(\theta_f, \dot{\theta}_f) = \mu(\tau_m + \tau_d) \tag{4}$$

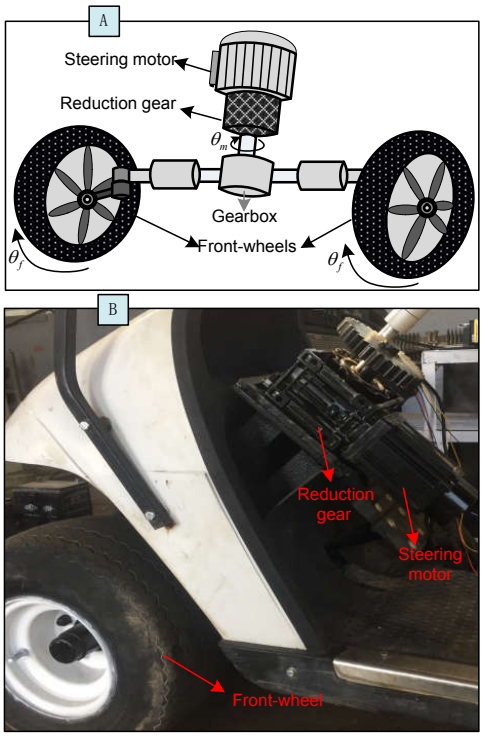

Fig. 2 Schematic diagram of the SbW system. (a) Schematic diagram of the SbW system, (b) Physical diagram of the SbW system.

with $\mathcal{J}_e = \mathcal{J}_f + \mu^2\mathcal{J}_m$. For brevity, the dynamics model (4) can be rewritten as

$$\begin{cases} \dot{x}_1 = x_2 \\ \dot{x}_2 = f_o(x_o) + gu + d_o(t) \\ y = x_1 \end{cases} \tag{5}$$

where $x_o = [x_1, x_2]^T = [\theta_f, \dot{\theta}_f]^T \in \mathbb{R}^2$, u is the real control input which is represented as τ_m in (4), $f_o(x_o) = -(\mu^2\mathcal{B}_m x_2 + \mathcal{H}_f(x))/\mathcal{J}_e$ denotes the lumped uncertain nonlinearity of the SbW system, $g = \mu/\mathcal{J}_e$, and $d_o(t) = \mu\tau_d/\mathcal{J}_e$ denotes the lumped motor pulsation disturbance [9, 10].

Control Objective: This paper addresses the event-triggered output feedback control problem for SbW systems, such that

(1) the tracking error between the front-wheels steering angle and its reference signal can converge to the prespecified neighborhood of the origin in fixed time, and
(2) the jumping phenomenon of the control input caused by event-triggered communication can be eliminated.

The following assumptions are made on the reference signal and external disturbance, respectively.

Assumption 1 *The reference signal $y_d(t)$ is known, and there exist unknown positive constants $\bar{y}_d$ and $\bar{\dot{y}}_d$ such that $|y_d(t)| \leq \bar{y}_d$ and $|\dot{y}_d(t)| \leq \bar{\dot{y}}_d$.*

Table 4 Variables and parameters of SbW systems

Symbol	Model variable
$\mathcal{B}_m$	Viscous friction coefficient of steering motor assembly
$\mathcal{J}_m$	Rotational inertia of steering motor assembly
$\mathcal{J}_f$	Rotational inertia of front-wheels
$\mathcal{J}_e$	Rotational inertia of equivalent system
θ_m	Steering motor assembly steering angle
θ_f	Front-wheels steering angle
τ_m	Output torque of steering motor assembly
μ	Steering motor assembly angle/front-wheels angle
τ_{12}	Load torque of steering motor assembly
τ_s	Input torque on the steering arm
τ_e	Self-aligning torque of the front-wheels
τ_f	Friction torque
τ_d	Motor torque pulsation disturbance [9, 10]
β	Slip angle
γ	yaw rate
C_f	Front wheel cornering stiffness
C_r	Rear wheel cornering stiffness
v	longitudinal velocity
m	Vehicle mass
I_z	Polar moment of inertia
l_f	Distance from mass center to front axle
l_r	Distance from mass center to rear axle
t_m	Mechanical trails
t_p	Pneumatic trails
ρ_τ	Coefficient for various road conditions

Assumption 2 *There exists an unknown positive constant $\bar{d}$ such that $|\dot{d}(t)| \leq \bar{d}$.*

Assumption 3 *Considering the SbW system* (5)*, assume that $f_0(x_o)$ is first-order differentiable.*

Remark 1 : The above assumptions are relatively general, even compared with the existing researches on time-triggered tracking control of SbW systems [9–13]. Specifically, 1) for the assumption of the external disturbance $d(t)$, the same assumption as Assumption 2 can be found in [9–12]. Moreover, the assumptions that both the external disturbance and its time derivative are bounded is made in [15]. 2) for the assumption of the reference signal $y_d(t)$, both the time derivative of the reference signal $\dot{y}_d(t)$ and its second-order time derivative $\ddot{y}_d(t)$ are required in the control design [9–13]. It is worth noting that to ensure driving safety and vehicle comfort, the reference path is usually smooth and its change rate is usually bounded in the practice application. Thereby, we can find that the time derivative of the reference signal, i.e., $\dot{y}_d(t)$, may not be known but can be considered bounded in this context. So compared with the related works, e.g., [9–13], Assumptions 1-2 are rather mild.

In [7, 10, 46], the self-aligning torque τ_e can be obtained

$$\tau_e = -C_f(t_m + t_p)\left(\beta + \frac{\gamma l_f}{v} - \delta_{fw}\right) \tag{6}$$

where β and γ can be obtained from the following the two-degree-of-freedom model of the vehicle

$$\begin{bmatrix}\dot{\beta}\\ \dot{\gamma}\end{bmatrix} = \begin{bmatrix}\frac{-C_f-C_r}{mv} & -1+\frac{C_r l_r - C_f l_f}{mv^2}\\ \frac{C_r l_r - C_f l_f}{I_z} & \frac{-C_f l_f^2 - C_r l_r^2}{I_z v}\end{bmatrix}\begin{bmatrix}\beta\\ \gamma\end{bmatrix} + \begin{bmatrix}\frac{C_f}{mv}\\ \frac{C_f l_f}{I_z}\end{bmatrix}\theta_f$$

where the parameters of the model are defined in Table 4.

Besides, the following simplified model of self-aligning torque can be obtained [9, 11, 47, 48]

$$\tau_e = \rho_\tau \tanh(x_1) \tag{7}$$

where ρ_τ denotes a time-varying coefficient for various road conditions, and θ_f means the steering angle of the front-wheels. From (6)-(7), one can find that τ_e is first-order differentiable.

Furthermore, the SbW system is a typical electromechanical system that can be expressed by the general EulerLagrange formulation. According to the existing researches [49, 50], the friction torque τ_f can be presented as the following parameterized form

$$\begin{aligned}\tau_f =& \alpha_1(\tanh(\beta_1 x_2) - \tanh(\beta_2 x_2)) + \alpha_2 \tanh(\beta_3 x_2)\\ &+ \alpha_3 x_2\end{aligned} \tag{8}$$

with α_i and β_i, $i = 1, 2, 3$ being the positive constants to be defined, which means that τ_f is differentiable.

From the above analysis, one can find that the self-aligning torque τ_e and friction torque τ_f of SbW systems are first-order differentiable, i.e., the nonlinearity $f_0(x_0)$ of (5) is differentiable. From a practical point of view, the self-aligning torque τ_e and friction torque τ_f of SbW systems have physical meaning. So their rate of change exists and is continuous. Therefore, the assumption that the nonlinearity of the SbW system is first-order differentiable is true in practice.

2.2 Fuzzy logic system and Useful Lemmas

A typical FLS consists of four parts: knowledge base, fuzzifier, fuzzy inference engine and defuzzifier. The

Table 5 Sufficient condition of finite-time stability and its residual seta and settling time

Reference	Sufficient condition	Residual set	Setting time
Zhu et al. [53]	$\dot{V}(x) \leq -cV^{\beta}(x) + \varepsilon$ with $c, \varepsilon > 0$, $1 > \beta > 0$.	$V(x) \leq \left[\frac{\varepsilon}{(1-\varsigma)c}\right]^{\frac{1}{\beta}}$, with $1 > \varsigma > 0$.	$T \leq \frac{V^{1-\beta}(0)}{c\varsigma(1-\beta)}$ with $1 > \varsigma > 0$.
Yu et al. [54]	$\dot{V}(x) \leq -\lambda_1 V(x) - \lambda_2 V^{\gamma}(x) + \eta$, with $\lambda_i, \eta > 0$, $1 > \gamma > 0$.	$V(x) \leq \min\left\{\frac{\eta}{(1-\varsigma)\lambda_1}, \left(\frac{\eta}{(1-\varsigma)\lambda_2}\right)^{\frac{1}{\gamma}}\right\}$, with $1 > \varsigma > 0$.	$T \leq \frac{1}{\lambda_1(1-\gamma)} \max\{ \frac{1}{\varsigma} \times \ln\left(1 + \frac{\varsigma\lambda_1 V^{1-\gamma}(0)}{\lambda_2}\right), \ln\left(1 + \frac{\lambda_1 V^{1-\gamma}(0)}{\varsigma\lambda_2}\right)$

knowledge base consists of a series of fuzzy IF-THEN inference rules:

$$\mathcal{R}_j : \text{IF } \chi_1 \text{ is } \mathcal{F}_1^j \cdots \text{and } \chi_n \text{ is } \mathcal{F}_n^j, \text{THEN } \mathcal{Y} \text{ is } \mathcal{G}^j, j = 1, \cdots, m$$

where χ_l, $l = 1, \cdots, n$, and $\mathcal{Y}$ denote the inputs and output of FLS, respectively, $\mathcal{F}_l^j$ and $\mathcal{G}^j$ are fuzzy sets and their membership functions are $\mu_{\mathcal{F}_l^j}(\chi_l)$ and $\mu_{\mathcal{G}^j}(\mathcal{Y})$, respectively, m is the number of fuzzy rules. Then, through the singleton fuzzifier, center average defuzzification, and product inference, the output of FLS can be expressed as

$$\mathcal{Y} = \Theta^T \xi(\chi) \tag{9}$$

where $\Theta = [\Theta_1, \cdots, \Theta_m]^T = [\Phi_1, \cdots, \Phi_m]^T$ with $\Phi_j = \max_{\mathcal{Y} \in \mathbb{R}} \mu_{\mathcal{G}^j}(\mathcal{Y})$ is the parameter vector, and the fuzzy basis function vector is $\xi(\chi) = [\xi^1(\chi), \cdots, \xi^m(\chi)]^T$ with

$$\xi^j(\chi) = \prod_{l=1}^{n} \mu_{\mathcal{F}_l^j}(\chi_l) / \sum_{j=1}^{m} \prod_{l=1}^{n} \mu_{\mathcal{F}_l^j}(\chi_l) \tag{10}$$

Lemma 1 *(see[51]) Suppose that the input universe of discourse Ω is a compact set in $\mathbb{R}^n$. Then, for the continuous function $f(\chi)$ on Ω and arbitrary $\bar{\omega} > 0$, there exists an FLS (9) with an optimal parameter vector Θ^* such that*

$$|\Theta^{*T} \xi(\chi) - f(\chi)| \leq \bar{\omega}. \tag{11}$$

Lemma 2 *(see[52]) Consider a class of systems $\dot{x} = f(x)$, there exist a smooth positive-definite function $V(x)$ and some positive scalars $\alpha > 0$, $\beta > 0$, $p > 0$, $p > 0$ and $k > 0$ such that*

$$\dot{V}(x) \leq -[\alpha V^p(x) + \beta V^q(x)]^k. \tag{12}$$

Then the fixed-time stability can be guranteed with the setting time $T_r \leq \frac{1}{\alpha^k(1-pk)} + \frac{1}{\beta^k(qk-1)}$.

Lemma 3 *Consider a class of systems $\dot{x} = f(x)$, there exist a smooth positive-definite function $V(x)$ and some positive scalars $\alpha_1 > 0$, $\alpha_2 > 0$, $\alpha_3 > 0$, $1 > \beta_1 > 0$, and $1 > \beta_2 \geq 0$ such that*

$$\dot{V}(x) \leq -\alpha_1 V(x) - \alpha_2 V^{\beta_1}(x) + \alpha_3 V^{\beta_2}(x) \tag{13}$$

then system $\dot{x} = f(x)$ is semi-global practical finite-time stable, i.e., the following inequality can be obtained if $t \geq T_r$

$$V(x) \leq \begin{cases} \left[\frac{\alpha_3}{(1-\varsigma)\alpha_1}\right]^{\frac{1}{1-\beta_2}}, & \text{if } \beta_1 \leq \beta_2 \\ \min\left\{\left[\frac{\alpha_3}{(1-\varsigma)\alpha_1}\right]^{\frac{1}{1-\beta_2}}, \left[\frac{\alpha_3}{(1-\varsigma)\alpha_2}\right]^{\frac{1}{\beta_1-\beta_2}}\right\}, & \text{else} \end{cases}$$

where $1 > \varsigma > 0$ and T_r is bounded as

$$T_r \leq \begin{cases} T_0 + \frac{1}{\varsigma\alpha_1(1-\beta_1)} \ln \frac{\varsigma\alpha_1 V^{1-\beta_1}(T_0) + \alpha_2}{\alpha_2}, & \text{if } \beta_1 \leq \beta_2 \\ T_0 + \max\left\{\frac{1}{\varsigma\alpha_1(1-\beta_1)} \ln \frac{\varsigma\alpha_1 V^{1-\beta_1}(T_0) + \alpha_2}{\alpha_2}, \right. \\ \left. \frac{1}{\alpha_1(1-\beta_1)} \ln \frac{\alpha_1 V^{1-\beta_1}(T_0) + \varsigma\alpha_2}{\varsigma\alpha_2}\right\}, & \text{else} \end{cases}$$

with T_0 being the initial time.

The proof of Lemma 3 is given in Appendix A.

Remark 2 To improve the closed-loop system's transient performance, finite-time control methods have been developed for various nonlinear systems during the past few years [53–55]. Generally, the practical finite-time stability of closed-loop systems can be guaranteed for uncertain nonlinear systems. As shown in Tab.5, the conclusion of practical finite-time stability theory can be obtained from the existing research. From Tab. 5, one can find that [53] provides a more general Lyapunov condition of the practical finite-time stability. However, consider the system $\dot{x} = f(x)$, if there exist continuous positive-definite function $V(x)$ and some scalars $\alpha_i > 0$, $i = 1, 2, 3$, $1 > \beta_1 > 0$, and $1 > \beta_2 \geq 0$ such that

$$\dot{V}(x) \leq -\alpha_1 V(x) - \alpha_2 V^{\beta_1}(x) + \alpha_3 V^{\beta_2}(x) \tag{14}$$

when $\beta_2 \neq 0$, the trajectory of system $\dot{x} = f(x)$ is difficult to judge based on the conclusions of [53] and [54]. This Lyapunov condition (i.e., $\beta_2 \neq 0$) is corresponds to the stability analysis of the state observer in this paper. Thus, the following Lemma is given in this paper.

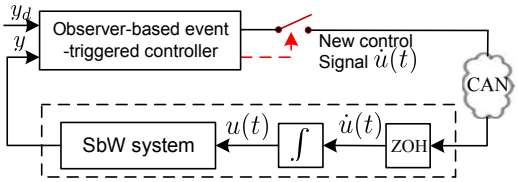

Fig. 3 Schematic diagram of proposed event-triggered control systems

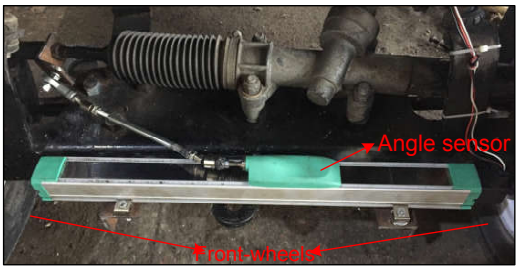

Fig. 4 The application of the angle sensor.

3 State Observer and Event-Triggered Control Design

3.1 Fuzzy-based state observer design

To eliminate the jumping phenomenon of control input, a new framework of the event-triggered control system, as shown in Fig.3, is proposed. In this context, based on [16, 56], the following augmented system (15) can be established from the system (5) by introducing the auxiliary variable $\zeta = u$

$$\begin{cases} \dot{x}_i = x_{i+1}, \ i = 1, 2 \\ \dot{x}_3 = f(x) + g\dot{u} + d(t) \\ y = x_1 \end{cases} \tag{15}$$

where $x = [x_1, x_2, x_3]^T$, $f(x) = \mathrm{d}f_o(x_o)/\mathrm{d}t$, $d(t) = \dot{d}_{ob}(t)$, $\dot{u}$ is considered as the "new" control signal to be designed.

As shown in Fig. 4, the angle position x_1 of the augmented system (15) can be measured by a linear sensor. In practical applications, the angular velocity of the front wheel's steering angle can be obtained through a sensor such as an encoder or gyroscope. However, the introduction of non-essential sensors will increase the hardware complexity and cost, thereby reducing the reliability of SbW systems. For this reason, the state observer is proposed for the augmented system (15), i.e.,

$$\begin{cases} \dot{\hat{x}}_i = -k_i\phi_i(\tilde{x}_1) + \hat{x}_{i+1}, \quad i = 1, 2 \\ \dot{\hat{x}}_3 = -k_3\phi_2(\tilde{x}_1) + \mathcal{Y} + g\dot{u} + \dot{\hat{d}}(t) \end{cases} \tag{16}$$

where $\chi = [x_1, \hat{x}_2, \hat{x}_3]^T$ and $\mathcal{Y} = \Theta^T\xi(\chi)$ denotes the input and output of FLS, $\tilde{x}_1 = \hat{x}_1 - x_1$, $\hat{d}(t)$ is the estimation of the disturbance $d(t)$, the parameters k_1, k_2 and k_3 satisfy that $A = [-k_1, 1, 0; -k_2, 0, 1; -k_3, 0, 0]$ is Hurwitz, $\phi_1(\tilde{x}_1) = (\mu_1 + \mu_2|\tilde{x}_1|)^{3/4}\lfloor\tilde{x}_1\rceil^0 + \tilde{x}_1$, $\phi_2(\tilde{x}_1) = \phi_1(\tilde{x}_1)\phi_1'(\tilde{x}_1)$, with $\mu_1, \mu_2 > 0$, and

$$\phi_1'(\tilde{x}_1) = \frac{3\mu_2}{4}(\mu_1 + \mu_2|\tilde{x}_1|)^{-\frac{1}{4}} + 1 \tag{17}$$

Besides, the adaptive laws of Θ and $\hat{d}(t)$ are designed as

$$\dot{\Theta} = \gamma_1\psi(S)\xi(\chi) - \sigma_1\Theta \tag{18}$$

$$\dot{\hat{d}}(t) = \gamma_2\psi(S) - \sigma_2\hat{d}(t) \tag{19}$$

where $\psi(\tilde{x}_1) = -\flat(t)\phi_1(\tilde{x}_1)/(|\phi_1(\tilde{x}_1)| + \varepsilon_{ob})$, σ_1, σ_2, γ_1, γ_2 and ε_{ob} are positive constants, and $\flat(t)$ with $\flat_{ob} > 0$ is

$$\flat(t) = \begin{cases} \sin\left(\dfrac{\pi t}{2\epsilon}\right), & \text{if } |t| < \flat_{ob} \\ 1, & \text{else} \end{cases} \tag{20}$$

For the adaptive state observer (16), the following main results can be obtained in this section.

Lemma 4 *Consider the adaptive laws* (18)-(19)*, there exist unknown positive constants* $\bar{\bar{\Theta}}$ *and* $\bar{\bar{d}}$ *such that* $\|\tilde{\Theta}\| \le \bar{\bar{\Theta}}$ *and* $|\tilde{d}| \le \bar{\bar{d}}$*,* $\forall t > 0$ *with* $\tilde{\Theta} = \Theta - \Theta^*$ *and* $\tilde{\bar{d}} = \hat{d} - d$*. Moreover, there also exist* $\bar{\Theta} \ge \|\Theta\|$ *for* $t > 0$*.*

The proof of Lemma 4 is given in Appendix B.

Theorem 1 *Consider the observer* (16)*, if parameters meet* $\lambda_{\min}(Q) - 3\mu_2\|B_1P\|(2\mu_1^{1/4})^{-1} \ge \kappa_{ob}$ *with* $B_1 = [0, 1, 0]^T$*, the estimation error of state can converge to the small neighborhood of the origin in finite time. i.e.,*

$$\|\hat{x} - x\| \le \mathcal{C}_{ob}, \ \forall t \ge T_{ob} \tag{21}$$

with $\mathcal{C}_{ob} = \max(\frac{\mu_1}{\lambda_{\min}(Q)}, \mathcal{C}_{o1})/\lambda_{\min}^{1/2}(P)$*, and*

$$T_{ob} \le \max\left\{\frac{8\lambda_{\max}(P)}{\varsigma\kappa_{ob}}\ln\left(1 + \frac{4(\lambda_{\min}(Q) + \mu_2)^{\frac{1}{4}}\kappa_{ob}\varsigma V_{ob}(0)}{3\mu_1\lambda_{\min}(Q)\lambda_{\max}^{\frac{7}{8}}(P)}\right), \right.$$
$$\left. \frac{8\lambda_{\max}P)}{\kappa_{ob}}\ln\left(1 + \frac{4(\lambda_{\min}(Q) + \mu_2)^{\frac{1}{4}}\kappa_{ob}V_{ob}(0)}{3\varsigma\mu_1\lambda_{\min}(Q)\lambda_{\max}^{\frac{7}{8}}(P)}\right)\right\}.$$

$$\mathcal{C}_{o1} = \min\left\{\left[\frac{2\bar{\Phi}\lambda_{\max}^2(P)}{(1-\varsigma)\kappa_{ob}}\right]^4, \left[\frac{8(\lambda_{\min}(Q) + \mu_2)^{\frac{1}{4}}\bar{\Phi}\lambda_{\max}^{\frac{15}{8}}(P)}{3\mu_1(1-\varsigma)\lambda_{\min}(Q)}\right]^{\frac{4}{3}}\right\}$$

where $P = P^T > 0$ *is the solution of* $A^TP + PA = -Q$ *with* Q *being the designed positive definite matrix,* $\bar{\Theta}$ *has been defined in Lemma 4,* $\bar{\Phi} = \bar{\Theta} + \|\Theta^*\| + \bar{\bar{d}} + \bar{\omega}$*,* $\bar{\omega}$ *has been defined in Lemma 1, and* $\bar{\bar{\Theta}}$ *and* $\bar{\bar{d}}$ *have been defined in Lemma 4.*

Proof : Combined with (5) and (16), the following dynamics of observation errors can be obtained

$$\begin{cases} \dot{\tilde{x}}_i = -k_i\phi_i(\tilde{x}_1) + \tilde{x}_{i+1}, \quad i = 1,2 \\ \dot{\tilde{x}}_3 = -k_3\phi_2(\tilde{x}_1) + \Phi(t) \end{cases} \tag{22}$$

where $\tilde{x} = [\tilde{x}_1, \tilde{x}_2, \tilde{x}_3]^T = [\hat{x}_1 - x_1, \hat{x}_2 - x_2, \hat{x}_3 - x_3]^T$ and $\Phi(t) = \Theta^T\xi(\chi) - \Theta^{*T}\xi(x) + \omega + \tilde{d}(t)$ with $\omega = \Theta^{*T}\xi(x) - f(x)$.

Consider the following Lyapunov function candidate

$$V_{ob} = \zeta^T P \zeta \tag{23}$$

where $\zeta = [\phi_1(\tilde{x}_1), \tilde{x}_2, \tilde{x}_3]^T$ and $P = P^T > 0$. Note that $\tilde{x}_1 \equiv 0$ means $\dot{\tilde{x}}_1 \equiv 0$ is also hold, and from (22), one can find that $V_{ob} \equiv 0$ will be always hold in this context. Thus the following analysis is given for the condition that $\tilde{x}_1 \neq 0$.

From (22), the following equation can be obtained

$$\begin{aligned} \dot{\zeta} =& \begin{bmatrix} \phi_1^{'}(\tilde{x}_1)(\tilde{x}_2 - k_1\phi_1(\tilde{x}_1)) \\ \phi_1^{'}(\tilde{x}_1)(\tilde{x}_3 - k_2\phi_1(\tilde{x}_1)) \\ -k_3\phi_1^{'}(\tilde{x}_1)\phi_1(\tilde{x}_1) \end{bmatrix} + \begin{bmatrix} 0 \\ (1 - \phi_1^{'}(\tilde{x}_1))\tilde{x}_3 \\ \Psi(t) \end{bmatrix} \\ =& \phi_1^{'}(\tilde{x}_1)A\zeta + B_1(1 - \phi_1^{'}(\tilde{x}_1))\tilde{x}_3 + B_2\Phi(t) \end{aligned} \tag{24}$$

with $B_1 = [0,1,0]^T$ and $B_2 = [0,0,1]^T$. Combined with (23) and (24), the derivative of V_{ob} can be obtained

$$\begin{aligned} \dot{V}_{ob} \leq& -\phi_1^{'}(\tilde{x}_1)\zeta^T Q\zeta + 2B_1^T P\zeta(1 - \phi_1^{'}(\tilde{x}_1))\tilde{x}_3 + 2PB_2\zeta\Psi(t) \\ \leq& -\kappa_{ob}\|\zeta\|^2 - \frac{3\mu_1\lambda_{\min}(Q)}{4(\lambda_{\min}(Q) + \mu_2)^{\frac{1}{4}}}\|\zeta\|^{\frac{7}{4}} + 2\lambda_{\max}(P)\bar{\Phi}\|\zeta\| \\ \leq& -\frac{\kappa_{ob}V_{ob}}{\lambda_{\max}(P)} - \frac{3\mu_1\lambda_{\min}(Q)V_{ob}^{\frac{7}{8}}}{4(\lambda_{\min}(Q) + \mu_2)^{\frac{1}{4}}\lambda_{\max}^{\frac{7}{8}}(P)} \\ & + 2\lambda_{\max}^{\frac{1}{2}}(P)\bar{\Phi}V_{ob}^{\frac{1}{2}} \end{aligned} \tag{25}$$

with $|\tilde{x}_3| \leq \|\zeta\|$, $|1 - \phi_1'(\tilde{x}_1)| \leq \frac{3\mu_2}{4\mu_2\mu_1^{1/4}}$, and $\phi_1^{'}(\tilde{x}_1) \geq \frac{3\mu_1}{4}\|\zeta\|^{-1/4}(\lambda_{\min}(Q) + \mu_2)^{-1/4} + 1$ if $\|\zeta\| \geq \mu_1/\lambda_{\min}(Q)$. This together with Lemma 3 yields

$$V_{ob} \leq \mathcal{C}_{ob}, \ \forall\ t \geq T_{ob}$$

This ends the proof of Theorem 1.

Remark 3 : As can be seen from Lemma 1, the approximation property of FLS can only be established in a convex region of interest, which implies that the initial states are within the bounded set. The same is true for all FLS/NN-based methods.

3.2 Event-triggered fixed-time control design

The following change of coordinates is given

$$z_1 = x_1 - y_d - \varrho_1 \tag{26}$$

$$z_2 = \hat{x}_2 + \eta_{11}z_1 - \varrho_2 \tag{27}$$

$$z_3 = \hat{x}_3 + \eta_{21}z_2 + \eta_{11}(\hat{x}_2 - \dot{y}_{r_1}) - \varrho_3 \tag{28}$$

where $\eta_{12} > 0$ and $\eta_{11},\ \eta_{21} > \frac{3}{2}$ are positive constants to be designed, $\varrho_i,\ i = 1,2,3$ can be obtained from following dynamics

$$\dot{\varrho}_i = \Psi_i[-\ell_i\varrho_i + \text{sign}(z_i)],\ \varrho_i(0) = 0, \quad i = 1,2,3 \tag{29}$$

with ℓ_1, ℓ_2 and τ_r being positive constants to be designed, and Ψ_1 and Ψ_2 being designed as

$$\Psi_1 = \eta_0(|z_1^3| + 2|z_1|z_2^2) + \eta_{12} + \kappa + \ell_2^{-1} + \Psi_1(t_k') + m_1 \tag{30}$$

$$\begin{aligned} \Psi_2 =& \eta_0(|z_2^3| + 2|z_2|z_3^2) + \eta_{22} + \ell_3^{-1} + k_2\phi_2(\kappa) + \kappa + \eta_{11}|\dot{\varrho}_1| \\ & + \Psi_2(t_k') + m_2 \end{aligned} \tag{31}$$

$$\begin{aligned} \Psi_3 =& \frac{gm + 2\delta|\Gamma|}{1 - \delta} + \eta_0(|z_3^3| + 2z_1^2|z_3|) + \eta_{32} + (\eta_{11} + \eta_{21}) \\ & \times k_2\phi_2(\kappa) + \eta_{11}\eta_{21}\kappa + \kappa + k_3\phi_2(\kappa) + \eta_{21}|\dot{\varrho}_2| \\ & + \Psi_3(t_k') + m_3 \end{aligned} \tag{32}$$

with $\Gamma = \Theta^T\xi(\chi) + \hat{d}(t) + (\eta_{11} + \eta_{21})\hat{x}_3 + \eta_{11}\eta_{21}\hat{x}_2$, and $\phi_2(\kappa) = \frac{3\mu_2}{4}(\mu_1 + \mu_2\kappa)^{\frac{1}{2}} + \frac{3\mu_2\kappa}{4}(\mu_1 + \mu_2\kappa)^{-\frac{1}{4}} + (\mu_1 + \mu_2\kappa)^{\frac{3}{4}} + \kappa$, where η_0, η_{12}, η_{22}, η_{32}, $1 > \delta > 0$ and m_i, $i = 1,2,3$ are positive constants to be designed, and Ψ_i, $i = 1,2,3$ can be obtained from the following updating mechanism

$$\Psi_i = \Psi_i(t_k'),\ \forall t \in [t_k', t_{k+1}') \tag{33}$$

$$t_{k+1}' = \{t > t_k' : |\Psi_i - \Psi_i(t_k')| \geq m_i\},\ t_1' = 0 \tag{34}$$

Moreover, the dynamic gain κ can be obtained from the following adaptive scheme

$$\dot{\kappa} = \kappa_d \text{sign}\left(\sum_{i=1}^{3} z_i^2\right),\ \kappa(0) = 0 \tag{35}$$

with κ_d being positive constant to be designed. Combined with (5), (16) and (29), one has

$$\begin{aligned} z_1\dot{z}_1 =& z_1[z_2 - \eta_{11}z_1 + \tilde{x}_2 - \dot{y}_d + \varrho_2 + \ell_2\varrho_1\Psi_1 - \Psi_1\text{sign}(z_1)] \\ \leq& -(\eta_{11} - \frac{1}{2})z_1^2 - \eta_{12}|z_1| + \frac{z_2^2}{2} + (|\tilde{x}_2| + \bar{\bar{y}}_d - \kappa)|z_1| \\ & - \eta_0(z_1^4 + 2z_1^2z_2^2) \end{aligned} \tag{36}$$

by combining with $|\varrho_2| \leq \ell_2^{-1}$ and $\Psi_1 \leq \Psi_1(t_k') + m_1$. From (16) and (29), one gets

$$\begin{aligned} z_2\dot{z}_2 =& z_2[-k_2\phi_2(\tilde{x}_1) + \hat{x}_3 + \eta_{11}(\hat{x}_2 + \tilde{x}_2 - \dot{y}_d) - \dot{\varrho}_2] \\ \leq& -(\eta_{21} - \frac{1}{2})z_2^2 - \eta_{22}|z_2| + \frac{z_3^2}{2} + \eta_{11}|z_2|(|\tilde{x}_2| + \bar{\bar{y}}_d - \kappa) \\ & + k_2|z_2|[|\phi_2(\tilde{x}_1)| - \phi_2(\kappa)] - \eta_0(z_2^4 + 2z_2^2z_3^2) \end{aligned} \tag{37}$$

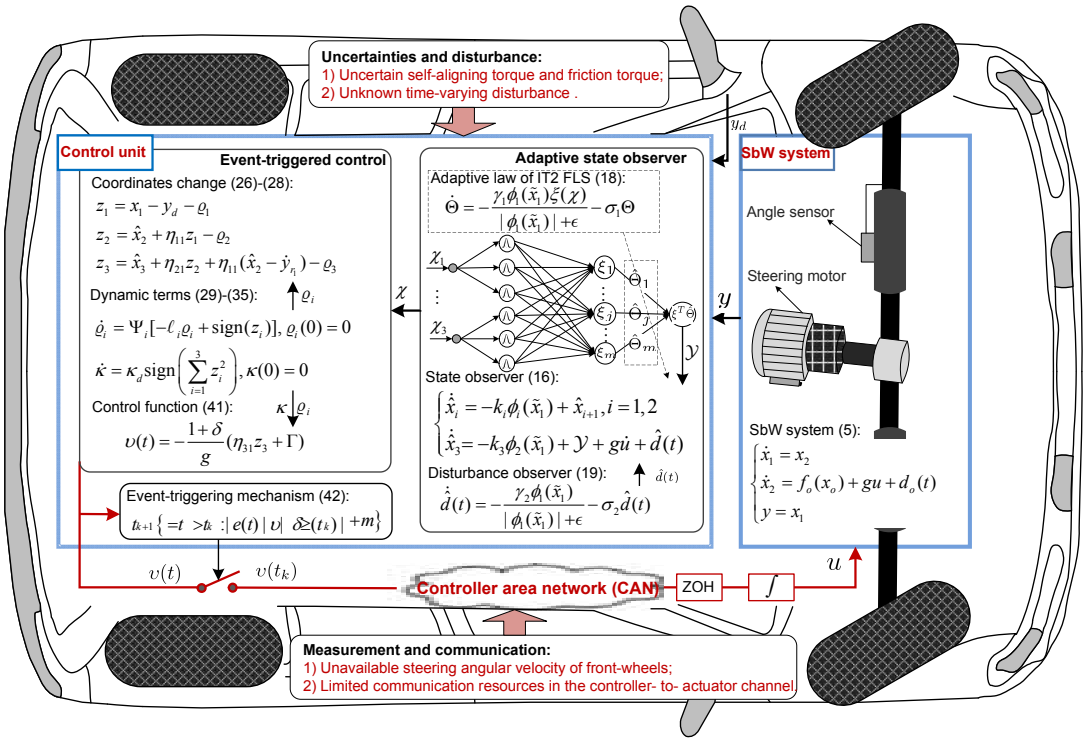

Fig. 5 The schematic of the observer-based event-triggered control of SbW systems.

by combining with $|\varrho_3| \le \ell_3^{-1}$ and $\Psi_2 \le \Psi_2(t_k')+m_2$. From (16), (28) and (29), one gets

$$\begin{aligned} z_3\dot{z}_3 = z_3[&-k_3\phi_2(\tilde{x}_1)+\Theta^T\xi(\chi)+g\dot{u}+\hat{d}(t)+(\eta_{11}+\eta_{21}) \\ &\times(\hat{x}_3-k_2\phi_2(\tilde{x}_1))+\eta_{11}\eta_{21}(\hat{x}_2+\tilde{x}_2-\dot{y}_d) \\ &+\eta_{21}\dot{\varrho}_2+\ell_3\Psi_3\varrho_3-\Psi_3\mathrm{sign}(z_3)] \end{aligned} \tag{38}$$

by combining with $\Psi_3 \le \Psi_3(t_k')+m_3$. As shown in Fig.5, the event-triggered control and the event-triggering mechanism of the augmented system (15) are designed as

$$\dot{u}(t) = \upsilon(t_k),\ \forall t \in [t_k, t_{k+1}) \tag{39}$$

$$t_{k+1} = \{t > t_k : |e(t)| \ge \delta|\upsilon(t_k)| + m\},\ t_1 = 0 \tag{40}$$

where $e = \upsilon(t) - \upsilon(t_k)$ denotes the event-triggered error and $\dot{u}(t) = \upsilon(t_k)$ denotes the "new" control signal with $\upsilon(t)$ being designed as

$$\upsilon(t) = -\frac{1+\delta}{g}(\eta_{31}z_3 + \Gamma) \tag{41}$$

with $\eta_{31} > \frac{3}{2}$ being positive constant to be designed.

Theorem 2 *Consider the augmented system* (15) *under the developed state observer* (16) *and event-triggered control* (39)*, the tracking error can converge to the prespecified neighborhood of the origin in fixed-time, i.e.,*

$$|y - y_d| \le \ell_1^{-1},\ \forall t \ge T_{tr} \tag{42}$$

where ℓ_1 *has been defined in* (29)*, and* T_{tr} *is defined as*

$$T_{tr} \le \frac{\max(\bar{\mathcal{C}} + \|\hat{x}(0)\|, \mathcal{C}_{ob})}{\kappa_d} + \frac{2}{c_2} + \frac{1}{\eta_0} \tag{43}$$

with $c_2 = \min(\eta_{12}, \eta_{22}, \eta_{32})$ *and* $\bar{\mathcal{C}} \ge \|x\|$ *for* $x \in \Omega$.

Proof : From the designed event-triggering mechanism (40), one can find that there exist $|\varsigma_i(t)| \le 1$ $(i = 1, 2)$ such that $\dot{u} = [\upsilon(t) + m\varsigma_2(t)]/[1 + \varsigma_1(t)\delta]$. This together with (31), (38) and (41) yields

$$\begin{aligned} z_3\dot{z}_3 \le &-(\eta_{31}-\frac{1}{2})z_3^2-\eta_{32}|z_3|+k_3(|\phi_2(\tilde{x}_1)|-\phi_2(\kappa))|z_3| \\ &+k_2(\eta_{11}+\eta_{21})(|\phi_2(\tilde{x}_1)|-\phi_2(\kappa))|z_3|+\eta_{11}\eta_{21} \\ &\times(|\tilde{x}_2|+\bar{\bar{y}}_d-\kappa)|z_3|-\eta_0(z_3^4+2z_1^2z_3^2). \end{aligned} \tag{44}$$

Consider the following Lyaponov function

$$V_{tr} = \frac{1}{2}\sum_{i=1}^{3} z_i^2. \tag{45}$$

The time derivative of V_{tr} along with (36), (37) and (44) can be obtained

$$\begin{aligned} \dot{V}_{tr} \le &-c_1V_{tr}-c_2V_{tr}^{\frac{1}{2}}-\eta_0V_{tr}^2+(|\tilde{x}_2|+\bar{\bar{y}}_d-\kappa)|z_1|+\eta_{11}|z_2| \\ &\times(|\tilde{x}_2|+\bar{\bar{y}}_d-\kappa)+k_2|z_2|[|\phi_2(\tilde{x}_1)|-\phi_2(\kappa)] \\ &+k_3(|\phi_2(\tilde{x}_1)|-\phi_2(\kappa))|z_3|+k_2(\eta_{11}+\eta_{21}) \\ &\times(|\phi_2(\tilde{x}_1)|-\phi_2(\kappa))|z_3|+\eta_{11}\eta_{21}(|\tilde{x}_2|+\bar{\bar{y}}_d-\kappa)|z_3| \end{aligned}$$

with $c_1 = \min(\eta_{11}, \eta_{21}, \eta_{31}) - 1$, $c_2 = \min(\eta_{12}, \eta_{22}, \eta_{32})$ and $z_1^4+z_2^4+z_3^4+2z_1^2z_2^2+2z_2^2z_3^2+2z_1^2z_3^2 = (z_1^2+z_2^2+z_3^2)^2$. Consider that $x \in \Omega$, there existing the positive constant $\bar{C}$ such that $\|x\| \leq \bar{\mathcal{C}}$. This together with the conclusion of Theorem 1 yields that $\|\tilde{x}\| \leq \max(\bar{\mathcal{C}} + \|\hat{x}(0)\|, \mathcal{C}_{ob})$ is always hold. Therefore, there exists a time instants T_0 that $\kappa(T_0) \geq \max(\bar{\mathcal{C}}+\|\hat{x}(0)\|, \mathcal{C}_{ob})+\bar{\bar{y}}_d$. Thus, the following dynamics can be obtained

$$\begin{aligned}\dot{V}_{tr} \leq & -c_1 V_{tr} - c_2 V_{tr}^{\frac{1}{2}} - \eta_0 V_{tr}^2 \\ \leq & -c_2 V_{tr}^{\frac{1}{2}} - \eta_0 V_{tr}^2. \end{aligned} \tag{46}$$

This together with Lemma 2 yileds that V can converge to the origin within fixed time with the setting time $T_{tr} \leq \frac{\max(\bar{\mathcal{C}}+\|\hat{x}(0)\|, \mathcal{C}_{ob})}{\kappa_d} + \frac{2}{c_2} + \frac{1}{\eta_0}$. This together with (26) yields

$$|y - y_d| \leq \ell_1^{-1}, \ \forall t \geq T_{tr} \tag{47}$$

This ends the proof of Theorem 2.

Remark 4 : In the practical application of the digital control system, the following dead-zone technique can be used to prevent the parameter drift problem of the adaptive law (35)

$$\dot{\kappa} = \kappa_d \max[0, \min(\text{sign}(V), \text{sign}(|z_1| - \varepsilon_c))] \tag{48}$$

where $\kappa(0) = 0$, ε_c is the small positive constant to be designed. Combined with (48) and the analysis of Theorem 2, it is not difficult to find that $V \leq \varepsilon_c$ can be achieved within fixed time. This together with (26) and (45) yields that

$$|y - y_d| \leq \ell_1^{-1} + \varepsilon_c \tag{49}$$

can be achieved in fixed time.

Remark 5 : In this paper, the contradiction method to prove that Zeno-behavior [57] is avoided. Suppose that $\Delta t_k = t_{k+1} - t_k = 0$. Due to the function $\upsilon(t)$ is always continuous, so one has

$$\lim_{\Delta t_k \to 0} |e(t_k + \Delta t_k)| = \lim_{\Delta t_k \to 0} |\upsilon(t_k + \Delta t_k) - \upsilon(t_k)| = 0. \tag{50}$$

However, it can be seen from (40) that

$$|e(t_k)| = \lim_{\Delta t_k \to 0} |e(t_k + \Delta t_k)| > m > 0. \tag{51}$$

The above analysis indicates that (50) contradicts the event-triggering condition (40), which means that the Zeno-behavior can be strictly avoided under the triggering mechanism (40).

4 Simulation and Experiment

4.1 Numerical simulation

(1). Simulation model of the SbW system

According to existing researches [10, 11], the friction torque τ_f in (4) are regarded as $\tau_f = 0.25(\tanh(100x_2) - \tanh(x_2)) + 30\tanh(100x_2) + 10x_2$, and self-aligning torque τ_e and the parameters of the system (4) can be easily obtained in [10]. The different stiffness coefficients and vehicle velocity with respect to τ_e are respectively used in the two simulations

$$\begin{cases} C_f = C_r = 80000, \ v = 5m/s, & \text{Simulation I} \\ C_f = C_r = 60000, \ v = 10m/s, & \text{Simulation II} \end{cases} \tag{52}$$

The initial condition of state is chosen as $[x_1(0), x_2(0)] = [0.1, 0]^T$, the disturbance is assumed as $d_{ob}(t) = 10\sin(2t)$, and the reference angle is considered as $y_d(t) = 5\int(y_m - y_d)\mathrm{d}t(\text{rad})$, with $y_m = 0.4\sin(0.8t)$, $\forall t \in [0, 10\pi)$; $y_m = 0.35\sin(0.6(t-10\pi))$, $\forall t \in [10\pi, 20\pi)s$; $y_m = 0.5\sin(0.4(t-20\pi))$, $\forall t \in [20\pi, 30\pi)s$; $y_m = 0.3\sin(0.8(t-30\pi))$, $\forall t \in [30\pi, 40\pi)s$; $y_m = 0.4\sin(0.4(t-40\pi))$, $\forall t \in [40\pi, 50\pi)s$; $y_m = 0.5\sin(0.2(t-50\pi))$, $\forall t \in [50\pi, 60\pi)s$; $y_m = 0.3\sin(0.4(t-60\pi))$, $\forall t \in [60\pi, 70\pi]s$.

(2). Parameter selection of the designed method

The parameters for the state observer (16)-(19) are selected as $\mu_1 = 0.2$, $\mu_2 = 0.1$, $k_1 = 1.3$, $k_2 = 15$, $k_3 = 15$, $\flat_{ob} = 0.01$, $\gamma_1 = 22600$, $\sigma_1 = 0.1$, $\gamma_2 = 1890$, $\sigma_2 = 0.1$, and $\varepsilon = 1$. The initial values $\Theta(0) = zeros(27, 1)$ and $\hat{d}(0) = 0$ are used. For FLS, the membership functions of the inputs are chosen as $\mu_{\mathcal{F}_i^j}(\chi_i) = \exp\left[-\frac{(\chi_i - 0.5(j-2))^2}{2\times 0.3^2}\right]$, $i = 1, 2, j = 1, 2, 3$ and $\mu_{\mathcal{F}_3^j}(\chi_3) = \exp\left[-\frac{(\chi_3 - 5(j-2))^2}{2\times 3^2}\right]$, $j = 1, 2, 3$ with the fuzzy set $\mathcal{F}_i^j$ of the inputs. The fuzzy IF-THEN rules are selected as shown in Tab.6, where

Table 6 The rule base of the fuzzy logic system

$\mathcal{Y}$ \ χ_2 / χ_3	χ_1 $\mathcal{F}_1^1$			$\mathcal{F}_1^2$			$\mathcal{F}_1^3$		
	$\mathcal{F}_2^1$	$\mathcal{F}_2^2$	$\mathcal{F}_2^3$	$\mathcal{F}_2^1$	$\mathcal{F}_2^2$	$\mathcal{F}_2^3$	$\mathcal{F}_2^1$	$\mathcal{F}_2^2$	$\mathcal{F}_2^3$
$\mathcal{F}_3^1$	$\mathcal{G}^1$	$\mathcal{G}^4$	$\mathcal{G}^7$	$\mathcal{G}^{10}$	$\mathcal{G}^{13}$	$\mathcal{G}^{16}$	$\mathcal{G}^{19}$	$\mathcal{G}^{22}$	$\mathcal{G}^{25}$
$\mathcal{F}_3^2$	$\mathcal{G}^2$	$\mathcal{G}^5$	$\mathcal{G}^8$	$\mathcal{G}^{11}$	$\mathcal{G}^{14}$	$\mathcal{G}^{17}$	$\mathcal{G}^{20}$	$\mathcal{G}^{23}$	$\mathcal{G}^{26}$
$\mathcal{F}_3^3$	$\mathcal{G}^3$	$\mathcal{G}^6$	$\mathcal{G}^9$	$\mathcal{G}^{12}$	$\mathcal{G}^{15}$	$\mathcal{G}^{18}$	$\mathcal{G}^{21}$	$\mathcal{G}^{24}$	$\mathcal{G}^{27}$

$\mathcal{G}^j$, $j = 1 \cdots 27$ are the fuzzy sets of the fuzzy output, and the center points of the sets $\mathcal{G}^j$ are defined as Θ_j with Θ_j being the j-th element of the vector Θ. The parameters of (26)-(41) and (48) are $\ell_1 = 2200$, $\ell_2 = 40$, $\ell_3 = 5$, $m_1 = m_2 = m_3 = 0.01$, $\kappa_d = 0.01$, $\eta_{11} = 80$,

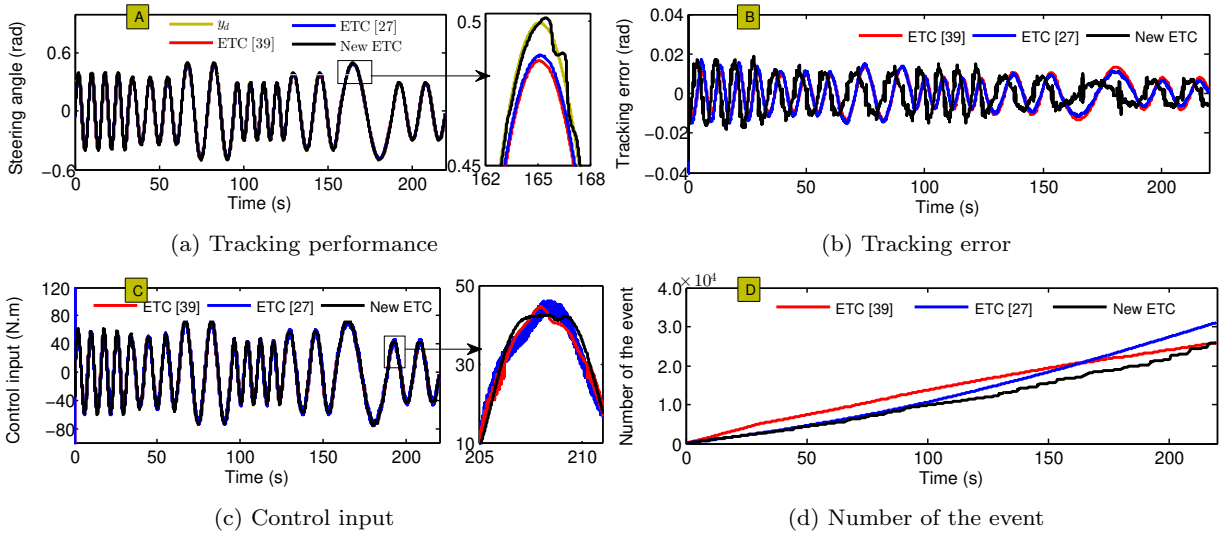

(a) Tracking performance (b) Tracking error

(c) Control input (d) Number of the event

Fig. 6 Control performance in the simulation I.

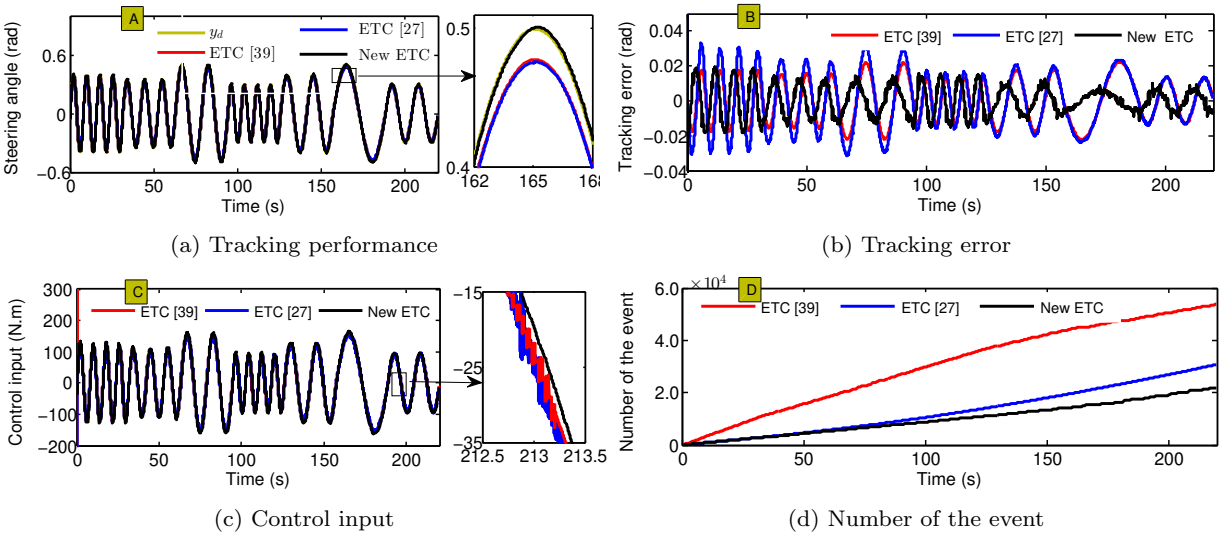

(a) Tracking performance (b) Tracking error

(c) Control input (d) Number of the event

Fig. 7 Control performance in the simulation II.

$\eta_{21}=70$, $\eta_{31}=60$, $\eta_{12}=\eta_{22}=\eta_{32}=0.1$, $m=18$, $\delta=0.2$ and $\varepsilon_c=0.04$.

(3). Parameter selection of the compared methods

To verify the adaptability and observation performance of the designed observer, the high-gain observer (HGO) designed in [25] is used to observe the system (15) for comparison, i.e.,

$$\dot{\hat{x}} = A_h\hat{x} + B_h f(\hat{x}) + L_h(y - C_h\hat{x}) \tag{53}$$

where $A_h=[0,1,0;0,0,1;0,0,0]$, $B_h=[0,0,1]^T$, $C=[1,0,0]$, and L_h is the observer gain vector. According to Theorem 3.2 and the equation (19) of [25], $L_h=[49,3918,35297]^T$ is chosen in simulation by solving matrix inequality (24) of [25].

The adaptive event-triggered control [39] and observer-based fuzzy event-triggered control [27] are chosen for comparison in this paper. For the SbW system (5), the adaptive state observer designed in [27] can be expressed as

$$\begin{cases} \dot{\hat{x}}_1 = \hat{x}_2 + k_1\phi_1(x_1 - \hat{x}_1) \\ \dot{\hat{x}}_2 = f(\hat{x}_2, u_f|\hat{\theta}) + u + k_2\phi_1(x_1 - \hat{x}_1) \end{cases} \tag{54}$$

where $\flat_1$ and $\flat_2$ satisfy that $A=[-k_1,1;-k_2,0]$ is Hurwitz, and $u_f = H_L(s)u$ with $H_L(s)$ being the Butterworth low-pass filters (as described in [27]). The event-triggered control designed in [27] can be expressed as

$$u(t) = r(t_k),\ \forall t \in [t_k, t_{k+1}) \tag{55}$$

$$t_{k+1} = \{t > t_k : |r(t) - u(t)| \geq \varrho_2\},\ t_1 = 0 \tag{56}$$

Table 7 Control performance in the simulation I

Index	Method	0∼10πs	10πs∼20πs	20πs∼30πs	30πs∼40πs	40πs∼50πs	50πs∼60πs	60πs∼70πs	0∼70πs
RMSE	ETC of [39]	0.0077	0.0066	0.0094	0.0057	0.0076	0.0094	0.0057	0.0076
	ETC of [27]	0.0104	0.0079	0.0100	0.0054	0.0066	0.0078	0.0044	0.0078
	New ETC	0.0097	0.0049	0.0054	0.0048	0.0034	0.0029	0.0031	0.0053
IAE	ETC of [39]	0.2142	0.1882	0.2666	0.1607	0.2152	0.2671	0.1623	1.4744
	ETC of [27]	0.2884	0.2223	0.2834	0.1527	0.1886	0.2200	0.1256	1.4810
	New ETC	0.3858	0.2531	0.2666	0.2435	0.1223	0.0955	0.1041	1.4720
NoE	ETC of [39]	5139	3758	4121	3693	3416	2834	2958	25919
	ETC of [27]	2700	3229	3882	4600	5061	5671	5877	31020
	New ETC	3122	3387	4106	4371	3541	2747	4606	25880

Table 8 Control performance in the simulation II

Index	Method	0∼10πs	10πs∼20πs	20πs∼30πs	30πs∼40πs	40πs∼50πs	50πs∼60πs	60πs∼70πs	0∼70πs
RMSE	ETC of [39]	0.0125	0.0110	0.0156	0.0093	0.0126	0.0157	0.0095	0.0126
	ETC of [27]	0.0214	0.0166	0.0213	0.0114	0.0142	0.0167	0.0095	0.0164
	New ETC	0.0107	0.0050	0.0061	0.0050	0.0037	0.0028	0.0028	0.0057
IAE	ETC of [39]	0.3518	0.3107	0.4433	0.2639	0.3569	0.4451	0.2684	2.4400
	ETC of [27]	0.6040	0.4698	0.6025	0.3233	0.4031	0.4724	0.2691	3.1442
	New ETC	0.4510	0.2735	0.3116	0.2638	0.1413	0.0814	0.0889	1.6510
NoE	ETC of [39]	10659	8580	8966	8808	6767	4834	5180	53794
	ETC of [27]	2838	3188	3756	4398	4957	5544	6051	30732
	New ETC	3443	3165	3279	3383	2884	2820	2919	21893

RMSE= $\sqrt{\frac{1}{n}\sum_{i=1}^{n} s_i^2}$, SD = $\sqrt{\frac{1}{n}\sum_{i=1}^{n}(s_i-\bar{s})^2}$, and IAE = $\int_0^t |s|\mathrm{d}t$ with $s = y - y_d$. NoE: Number of the event.

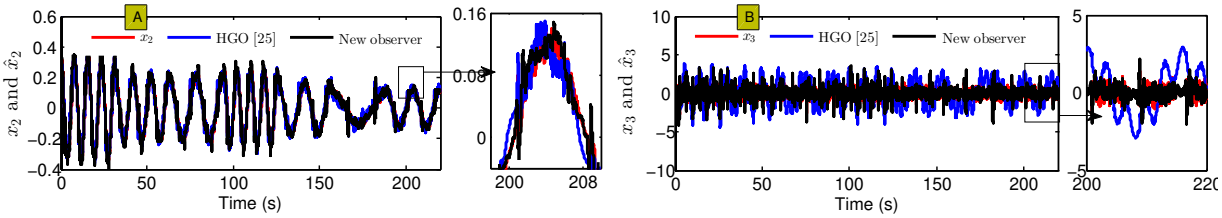

Fig. 8 Observation result in the simulation I. (a) State variable x_2 and its observation $\hat{x}_2$, (b) State variable x_3 and its observation $\hat{x}_3$.

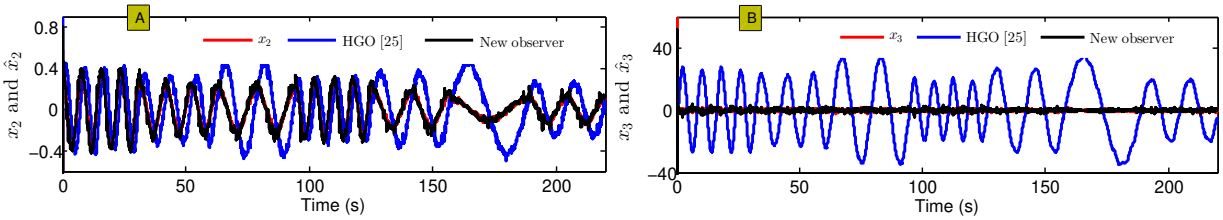

(a) State variable x_2 and its observation $\hat{x}_2$ (b) State variable x_3 and its observation $\hat{x}_3$

Fig. 9 Observation result in the simulation II.

with $\varrho_2 > 0$, and $r(t)$ being designed as $r(t) = \alpha_2(t) - \varrho_1 \tanh(\varsigma_2\varrho_1/\epsilon)$, where $\varrho_1 > \varrho_2 > 0$, $\epsilon > 0$, $\varsigma_2 = \hat{x}_2 - \alpha_1$, and α_1 and α_2 can be found in [27]. For the event-triggered control [27], the parameters of equations (7), (27)-(29), (31), (45), (46), (60), and (61) of [27] are chose as $c_1 = 5$, $c_2 = 10$, $k_1 = 5$, $k_2 = 2000$, $\omega_0 = 1.5$, $\omega_\infty = 0.8$, $\eta_{\max} = 0.5$, $\eta_{\min} = 0.4$, $\sigma = 0.01$, $\varepsilon = 0.1$, $\gamma_2 = 0.001$, $\varrho_1 = 1$, and $\varrho_2 = 2$. Besides, the event-triggered control with swithcing threshold strategy [39] can be expressed as

$$u(t) = \omega(t_k),\ \forall t \in [t_k, t_{k+1}) \tag{57}$$

$$t_{k+1} = \begin{cases} \{t > t_k : |e(t)| \geq \delta|u(t)| + m_1\},\ |u(t)| < D \\ \{t > t_k : |e(t)| \geq m\},\ |u(t)| \geq D \end{cases} \tag{58}$$

where $e(t) = u(t) - \omega(t)$ δ, m, m_1 and D are positive constants to be designed, and $\omega(t)$ being designed as

$$\omega(t) = \frac{1+\delta}{g}\left((\alpha_2 + \ddot{y}_d)\tanh(\frac{z_2(\alpha_2+\ddot{y}_d)}{\varepsilon} + m_1\tanh(\frac{m_1 z_2}{\varepsilon})\right)$$

where α_2 can be obtained from[39], and the related parameters in [39] are chosen as $c_1 = 180$, $\varphi_1 = 0$, $c_2 = 160$, $\varphi_2 = x_1$, $\Gamma = 1$, $\sigma = 0.1$, $\varepsilon = 1$, $\delta = 0.4$, $m = 0.2$, and $D = 30$.

(4). Simulation results and analysis

Fig. 6 and Tab. 7 give the control performance of the different ETCs in the simulation I. From Fig. 6 and Tab. 7, one can find that in the designed event-triggered control system, the tracking error can converge to the smaller residual set of the origin, and the jumping phenomenon of control input can be avoided while saving more communication resources. Fig. 7 and Tab. 8 give the control performance of the different ETCs in simulation II. One can find that the ETC designed in this paper also has better adaptability to model uncertainty. Fig. (8) and Fig. 9 give the observation results in simulation I and simulation II. From Fig. 8, one can find that both the designed adaptive state observer and model-based HGO can achieve satisfactory observation performance without model uncertainty. As shown in Fig. 9, when the model uncertainty is considered in simulation II, i.e., when the model parameters are changed, the observation performance of the adaptive observer designed in this paper is better than that of the model-based HGO.

4.2 Experiment

The experiment platform of SbW systems is shown in Fig. 10. In this platform, the single board computer (dSPACE-ds1202) is used as the control unit of SbW systems, and the servo motor driver (XiNJE DS2-20P7) is used for driving the steering motor (XiNJE MS80ST-M02430B-20P7) equipped with a reducer. The linear sensor (KTR11-10) fixed on the steering arm measures the steering angle of the front-wheels. A computer is applied to display the experimental results of the experiment on-line and store the experimental data. The sampling period is chosen as $0.001s$.

(1). Parameter selection of the proposed method

The parameters for the state observer (16)-(19) are selected as $\mu_1 = 0.5$, $\mu_2 = 0.1$, $k_1 = 5$, $k_2 = 15$, $k_3 = 10$, $\flat_{ob} = 0.2$, $\gamma_1 = 360$, $\sigma_1 = 0.01$, $\gamma_2 = 120$, $\sigma_2 = 0.01$, $\varepsilon = 0.1$, and $Q = diag(10^5, 0^5, 0^5)$. The initial values $\Theta(0) = zeros(27, 1)$ and $\hat{d}(0) = 0$ are used. For the fuzzy logic system, the membership function and fuzzy rule base are the same as those in simulation. The parameters of

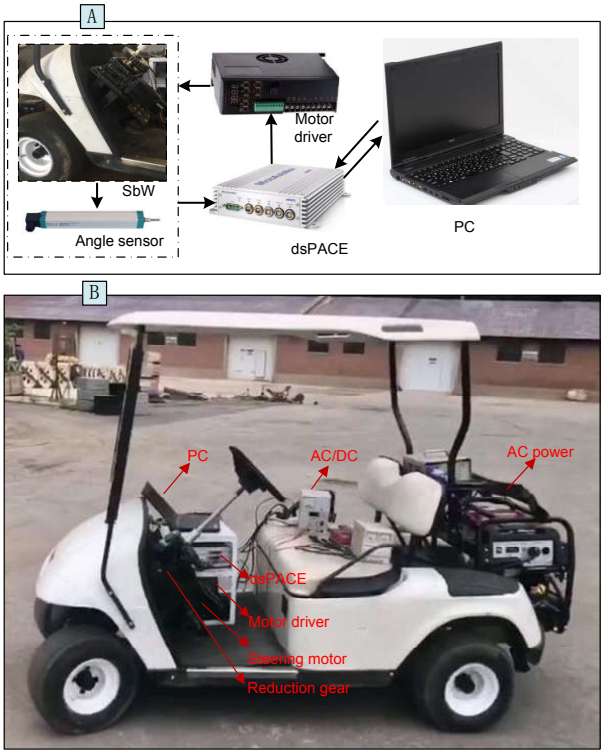

Fig. 10 The experiment platform of the SbW system. (a) Schematic diagram of the experiment platform, (b) Physical diagram of the experiment platform.

(26)-(41) and (48) are $\ell_1 = 120$, $\ell_2 = 10$, $\ell_3 = 2$, $m_1 = m_2 = m_3 = 0.01$, $\kappa_d = 0.01$, $\eta_{11} = 40$, $\eta_{21} = 15$, $\eta_{31} = 30$, $\eta_{12} = \eta_{22} = \eta_{32} = 0.1$, $m = 15$, $\delta = 0.1$ and $\varepsilon_c = 0.06$. To verify the robustness of the designed controller to time-varying disturbance, $u_{real} = u + d_e(t)$ is considered as the real control input of the SbW system with u being the designed control input. Besides, the following cases are considered

$$\begin{cases} d_e(t) = 5\cos(2t), \ v = 2m/s, & \text{Experiment I} \\ d_e(t) = 2\sin(4t), \ v = 5m/s, & \text{Experiment II} \end{cases} \tag{59}$$

(2). Parameter selection of the compared methods

To verify the adaptability and superiority of the designed observer, HGO [25] is used to estimate the system (15) for comparison in experiment. According to Theorem 3.2 and the equation (19) of [25], $L_h = [14.16, 339.4, 7965.86]^T$ is chosen in experiment by solving matrix inequality (24) of [25]. Besides, the following low-pass filter [21] is used for comparison

$$\tau\dot{\hat{x}} = x(t) - \hat{x} \tag{60}$$

where $\dot{\hat{x}}$ is the estimation of $\dot{x}$ and τ is the small positive constant to be designed. $\tau = 0.005$ is chosen in experiment.

To verify the jumping phenomenon of control input caused by the event-triggered communication can

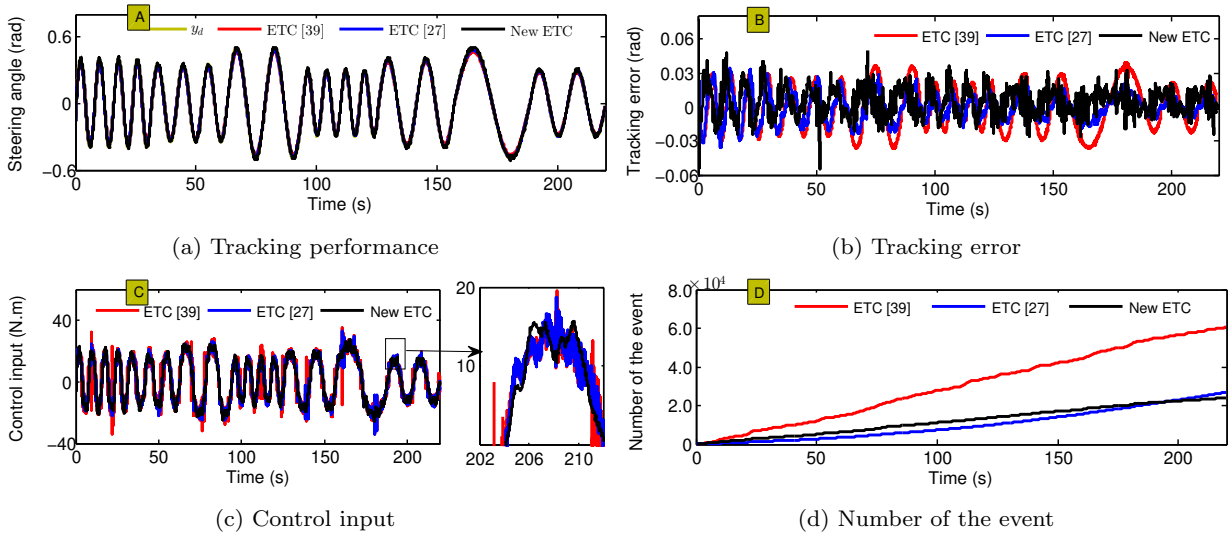

(a) Tracking performance (b) Tracking error

(c) Control input (d) Number of the event

Fig. 11 Control performance in experiment I.

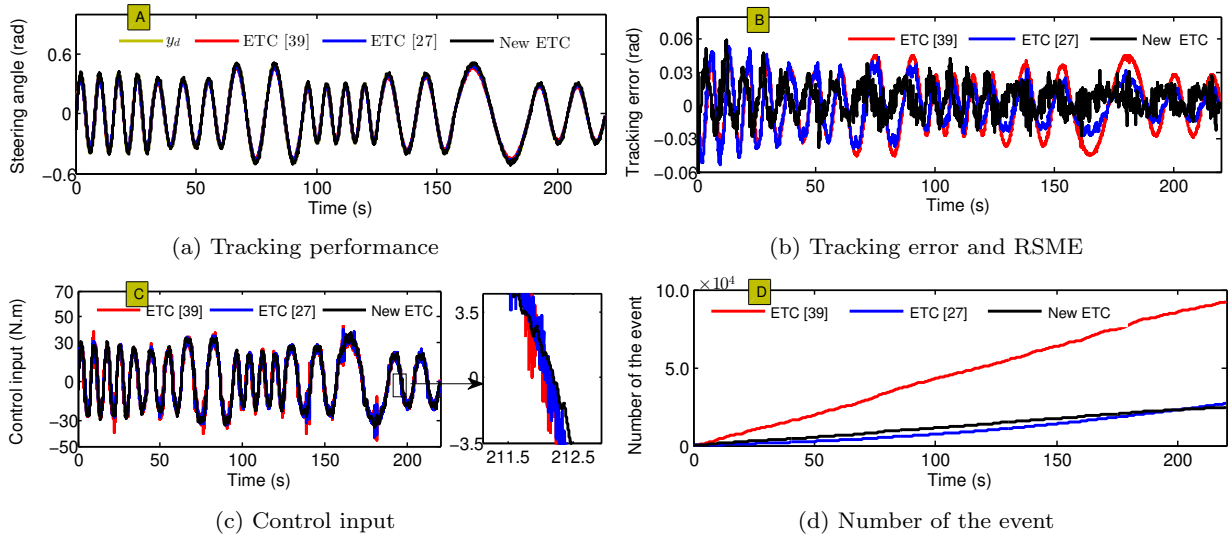

(a) Tracking performance (b) Tracking error and RSME

(c) Control input (d) Number of the event

Fig. 12 Control performance in experiment II.

be eliminated under the designed event-triggered control system, the adaptive event-triggered control [39] and observer-based fuzzy event-triggered control [27] are chosen for comparison. For the event-triggerid control [39], the parameters and functions of the equations (5), (7), (21), (22) and (28) of [39] are chosen as $c_1 = 20$, $\varphi_1 = 0$, $c_2 = 35$, $\varphi_2 = x_1$, $\Gamma = 1$, $\sigma = 0.1$, $\varepsilon = 1$, $\delta = 0.4$, $m = 0.2$, and $D = 20$. For the event-triggered control [27], the parameters of equations (7), (27)-(29), (31), (45), (46), (60), and (61) of [27] are chose as $c_1 = 10$, $c_2 = 25$, $k_1 = 1$, $k_2 = 200$, $\omega_0 = 2$, $\omega_\infty = 1$, $\eta_{\max} = 0.8$, $\eta_{\min} = 0.6$, $\sigma = 0.01$, $\varepsilon = 1$, $\gamma_2 = 0.001$, $\varrho_1 = 5$, and $\varrho_2 = 2$.

(3).Experiment results and analysis

Fig.11 and Tab.9 give control results in experiment I under the different ETCs. It is easy to find that in the designed event-triggered control system, the tracking error can converge to the smaller neighborhood of the origin, and the jumping phenomenon of control input caused by event-triggered communication can be avoided while saving more communication resources can be saved. Fig.12 and Tab.10 give control results in experiment II. It also can be found that the designed ETC can achieve better tracking accuracy, and the control input is without jumping phenomenon. Fig. 13 and Fig.14 give the observation result of the state x_2 and x_3 under the different experiments. From Fig. 13 and Fig.14, one can find that the estimation results under

Table 9 Control performance in the experiment I

Index	Method	0∼10πs	$10\pi s\sim20\pi s$	$20\pi s\sim30\pi s$	$30\pi s\sim40\pi s$	$40\pi s\sim50\pi s$	$50\pi s\sim60\pi s$	$60\pi s\sim70\pi s$	$0\sim70\pi s$
RMSE	ETC of [39]	0.0201	0.0175	0.0251	0.0138	0.0199	0.0252	0.0150	0.0200
	ETC of [27]	0.0202	0.0139	0.0152	0.0085	0.0091	0.0102	0.0057	0.0127
	New ETC	0.0192	0.0122	0.0126	0.0132	0.0109	0.0089	0.0094	0.0127
IAE	ETC of [39]	0.5267	0.4744	0.6904	0.3476	0.5314	0.7001	0.4046	3.6752
	ETC of [27]	0.5535	0.3854	0.4106	0.2326	0.2419	0.2740	0.1482	2.2562
	New ETC	0.4789	0.3106	0.3234	0.3443	0.2860	0.2268	0.2437	2.2137
NoE	ETC of [39]	8296	7080	10786	9494	7952	10654	6449	60711
	ETC of [27]	1649	1971	2972	3635	4678	5596	6066	26567
	New ETC	3509	3082	3903	3712	3460	3762	2604	24032

Table 10 Control performance in the experiment II

Index	Method	0∼10πs	$10\pi s\sim20\pi s$	$20\pi s\sim30\pi s$	$30\pi s\sim40\pi s$	$40\pi s\sim50\pi s$	$50\pi s\sim60\pi s$	$60\pi s\sim70\pi s$	$0\sim70\pi s$
RMSE	ETC of [39]	0.0259	0.0223	0.0317	0.0189	0.0255	0.0317	0.0191	0.0255
	ETC of [27]	0.0334	0.0226	0.0254	0.0136	0.0152	0.0170	0.0095	0.0209
	New ETC	0.0232	0.0130	0.0129	0.0151	0.0111	0.0089	0.0096	0.0141
IAE	ETC of [39]	0.7230	0.6213	0.8879	0.5215	0.7107	0.8914	0.5299	4.8857
	ETC of [27]	0.9297	0.6350	0.7041	0.3823	0.4176	0.4796	0.2548	3.8031
	New ETC	0.5747	0.3386	0.3407	0.3944	0.2954	0.2272	0.2506	2.4216
NoE	ETC of [39]	12412	12830	15312	12452	13698	14997	10631	92332
	ETC of [27]	1682	1998	3022	3736	4617	5748	6212	27015
	New ETC	3616	3183	3877	3881	3592	3850	2686	24685

RMSE= $\sqrt{\frac{1}{n}\sum_{i=1}^{n} s_i^2}$, SD = $\sqrt{\frac{1}{n}\sum_{i=1}^{n}(s_i-\bar{s})^2}$, and IAE = $\int_0^t |s|\mathrm{d}t$ with $s = y - y_d$. NoE: Number of the event.

the state observer are more smooth and suitable for the design of the output feedback controller. Besides, one can also find that the trend of observation results under the designed state observer is more consistent with the estimation results of the low-pass filter than the model-based HGO.

5 Conclusion

This paper proposes an event-triggered fixed-time control for uncertain SbW systems by considering the bandwidth limitation of CAN. A new framework is proposed to eliminate the jumping phenomenon of the event-based control input. Then, an adaptive fuzzy-based state observer and disturbance observer are proposed to estimate the unavailable state and disturbance of the augmented SbW system . Furthermore, an adaptive event-triggered control is proposed for SbW systems by considering the effect of observation error and event-triggered error, such that the prespecified tracking performance can be guaranteed within fixed time. Finally, simulations and experiments are presented to evaluate the effectiveness and superiority of the proposed methods. Future research on the SbW control system will include the following aspects:

(1) Input saturation and output constraint of the SbW system should be addressed. In the practical application, the control input saturation of SbW systems, i.e., output torque saturation of the steering motor, often occurs due to hardware limitations, limiting the SbW system performance severely even leads to the SbW system instability. Besides, the output constraint of SbW systems, i.e., the steering angle constraint of the front-wheels, is inevitable. So, the input saturation and output constraint of SbW systems will be considered in the control design.
(2) The time delay phenomenon should be considered. In the practical application of the SbW system, the time delay phenomenon caused by measurement and communication is inevitable, which will be considered in future research on SbW control systems.

Appendix A: Proof of Lemma 3

Case 1 $\beta_1 \geq \beta_2$. In this case, the inequality (13) can be expressed as (61) or (62)

$$\dot{V}(x) \leq -\varsigma\alpha_1 V(x) - \iota\alpha_1 V(x) - \alpha_2 V^{\beta_1}(x) + \alpha_3 V^{\beta_2}(x) \quad (61)$$

$$\dot{V}(x) \leq -\alpha_1 V(x) - \varsigma\alpha_2 V^{\beta_1}(x) - \iota\alpha_2 V^{\beta_1}(x) + \alpha_3 V^{\beta_2}(x) \quad (62)$$

where $\varsigma > 0$ and $\iota > 0$ satisfies $\varsigma + \iota = 1$. From (61), the following inequality can be obtained if $\iota\alpha_1 V(x) - \alpha_3 V^{\beta_2}(x) > 0$

$$\dot{V}(x) \leq -\varsigma\alpha_1 V(x) - \alpha_2 V^{\beta_1}(x). \quad (63)$$

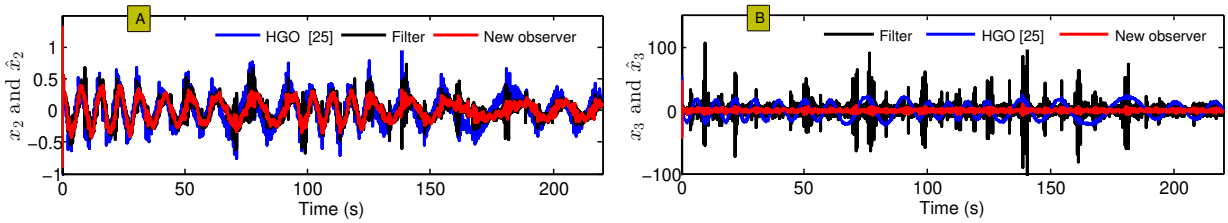

(a) State variable x_2 and its observation $\hat{x}_2$ (b) State variable x_3 and its observation $\hat{x}_3$

Fig. 13 Observation result in experiment I.

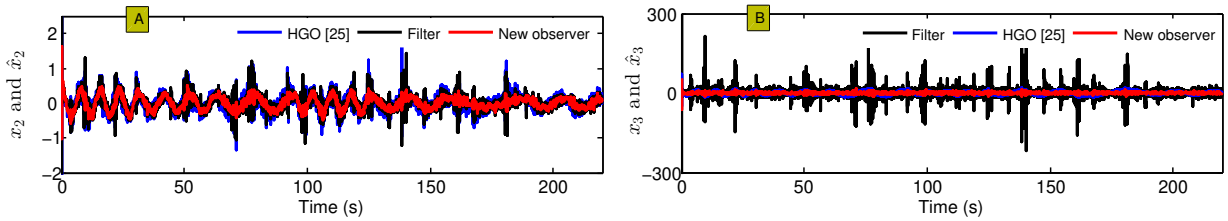

(a) State variable x_2 and its observation $\hat{x}_2$ (b) State variable x_3 and its observation $\hat{x}_3$

Fig. 14 Observation result in experiment II.

This together with *Corollary 1* of [54] yields

$$V^{1-\beta_2}(x) \leq \frac{\alpha_3}{(1-\varsigma)\alpha_1}, \ \forall\, t \geq T_{re_1} \tag{64}$$

with $T_{re_1} \leq T_0 + \frac{1}{\varsigma\alpha_1(1-\beta_1)} \ln \frac{\alpha_2+\varsigma\alpha_1 V^{1-\beta_1}(T_0)}{\alpha_2}$ and T_0 being the initial time. Similarly, from (62), one can get

$$V^{\beta_1-\beta_2}(x) \leq \frac{\alpha_3}{(1-\varsigma)\alpha_2}, \ \forall\, t \geq T_{re_2} \tag{65}$$

with $T_{re_2} \leq T_0 + \frac{1}{\alpha_1(1-\beta_1)} \ln \frac{\varsigma\alpha_2+\alpha_1 V^{1-\beta_1}(T_0)}{\varsigma\alpha_2}$. This completes the proof of Case 1 in Lemma 3.

Case 2 $\beta_1 < \beta_2$. In this case, the inequality (13) can be expressed as (61). Thus, the conclusion as in (64) can be obtained, which completes the proof of Case 2 in Lemma 3. This completes the proof of Lemma 3.

Appendix B: Proof of Lemma 4

From (18) one can get

$$\Theta^T\dot{\Theta} \leq -\sigma_1\|\Theta\|^2 + \gamma_1\|\Theta\| \tag{66}$$

with $|\psi(S)| \leq 1$ and $\|\xi(\chi)\| \leq 1$. Thus, it is not difficult to get that $\|\Theta\| \leq \bar{\Theta} = \max(\gamma_1/\sigma_1, \|\Theta\|(0))$. This together with the definition $\tilde{\Theta} = \Theta - \Theta^*$ yields $\|\tilde{\Theta}\| \leq \|\Theta^*\| + \bar{\Theta}$. Similarly, the estimation error $\tilde{d}$ is always bounded. This ends the proof of Lemma 4.

Conflict of interest statement

The authors have no conflicts of interest to declare that are relevant to the content of this article.

References

1. A. Kirli, Y. Chen, C. Okwudire, G. Ulsoy, Torque-vectoring-based backup steering strategy for steer-by-wire autonomous vehicles with vehicle stability control, IEEE Trans. Veh. Technol 68 (8) (2019) 7319–7328.
2. M. D. Vaio, P. Falcone, R. Hult, A. Petrillo, S. Santini, Design and experimental validation of a distributed interaction protocol for connected autonomous vehicles at a road intersection, IEEE Trans. Veh. Technol 68 (10) (2019) 9451–9465.
3. H. Peng, W. Wang, Q. An, C. Xiang, L. Li, Path tracking and direct yaw moment coordinated control based on robust mpc with the finite time horizon for autonomous independent-drive vehicles, IEEE Trans. Veh. Technol 69 (6) (2020) 6053–6066.
4. Z. Luan, J. Zhang, W. Zhao, C. Wang, Trajectory tracking control of autonomous vehicle with random network delay, IEEE Trans. Veh. Technol 69 (8) (2020) 8140–8150.
5. S. Tuohy, M. Glavin, C. Hughes, E. Jones, M. Trivedi, L. Kilmartin, Intra-vehicle networks: A review, IEEE Trans. Intell. Transp. Syst. 16 (2) (2015) 534–545.
6. R. Marino, S. Scalzi, M. Netto, Nested pid steering control for lane keeping in autonomous vehicles, Control Eng. Pract. 19 (12) (2011) 1459–1467.
7. P. Yih, J. Gerdes, Modification of vehicle handling characteristics via steer-by-wire, IEEE Trans. Control Syst. Technol. 13 (6) (2005) 965–976.

8. P. Falcone, F. Borrelli, J. Asgari, H. E. Tseng, D. Hrovat, Predictive active steering control for autonomous vehicle systems, IEEE Trans. Control Syst. Technol. 15 (3) (2007) 566–580.
9. H. Wang, H. Kong, Z. Man, D. M. Tuan, Z. Cao, W. Shen, Sliding mode control for steer-by-wire systems with ac motors in road vehicles, IEEE Trans. Ind. Electron. 61 (3) (2014) 1596–1611.
10. M. T. Do, Z. Man, C. Zhang, H. Wang, F. S. Tay, Robust sliding mode-based learning control for steer-by-wire systems in modern vehicles, IEEE Trans. Veh. Technol. 63 (2) (2014) 580–590.
11. Z. Sun, J. Zheng, Z. Man, H. Wang, Robust control of a vehicle steer-by-wire system using adaptive sliding mode, IEEE Trans. Ind. Electron. 63 (4) (2016) 2251–2262.
12. H. Wang, Z. Man, H. Kong, Y. Zhao, M. Yu, Z. Cao, J. Zheng, M. Do, Design and implementation of adaptive terminal sliding mode control on a steer-by-wire equipped road vehicle, IEEE Trans. Ind. Electron. 63 (9) (2016) 5774–5785.
13. X. D. Wu, M. M. Zhang, M. Xu, Active tracking control for steer-by-wire system with disturbance observer, IEEE Trans. Veh. Technol. 68 (6) (2019) 5483–5493.
14. C. Huang, F. Naghdy, H. Du, Delta operator-based fault estimation and fault-tolerant model predictive control for steer-by-wire systems, IEEE Trans. Control Syst. Technol. 26 (5) (2018) 1810–1817.
15. C. Huang, F. Naghdy, H. Du, Fault tolerant sliding mode predictive control for uncertain steer-by-wire system, IEEE Trans. Cybern 49 (1) (2019) 1810–1817.
16. A. Levant, Higher-order sliding modes, differentiation and output-feedback control, Int. J. Control 76 (9-10) (2003) 924–941.
17. A. Levant, M. Livne, Exact differentiation of signals with unbounded higher derivatives, IEEE Trans. Autom. Control 57 (4) (2012) 1076–1080.
18. J. Davila, L. Fridman, A. Levant, Second-order sliding-mode observer for mechanical systems, IEEE Trans. Autom. Control 50 (11) (2005) 1785–1789.
19. A. Apaza-Perez, J. A. Moreno, L. Fridman, Dissipative approach to sliding mode observers design for uncertain mechanical systems, Automatica 87 (2018) 330–336.
20. T. R. Oliveira, V. H. Pereira Rodrigues, L. Fridman, Generalized model reference adaptive control by means of global hosm differentiators, IEEE Trans. Autom. Control 64 (5) (2019) 2053–2060.
21. Y. Li, S. Tong, L. Liu, G. Feng, Adaptive output-feedback control design with prescribed performance for switched nonlinear systems, Automatica 80 (2017) 225–231.
22. K. D. V. Ellenrieder, Dynamic surface control of trajectory tracking marine vehicles with actuator magnitude and rate limits - sciencedirect, Automatica 105 (2019) 433–442.
23. S. Fatemeh, A. M. Mehdi, K. Alireza, K. H. Reza, Observer-based fuzzy adaptive dynamic surface control of uncertain nonstrict feedback systems with unknown control direction and unknown dead-zone, IEEE Trans. Syst., Man, Cybern., Syst. 49 (11) (2019) 2340–2351.
24. A. Alessandri, A. Rossi, Increasing-gain observers for nonlinear systems: Stability and design, Automatica 57 (2015) 180–188.
25. A. Zemouche, F. Zhang, F. Mazenc, R. Rajamani, High-gain nonlinear observer with lower tuning parameter, IEEE Trans. Autom. Control 64 (8) (2019) 3194–3209.
26. S. Tong, B. Huo, Y. Li, Observer-based adaptive decentralized fuzzy fault-tolerant control of nonlinear large-scale systems with actuator failures, IEEE Trans. Fuzzy Syst 22 (1) (2014) 1–15.
27. J. Qiu, K. Sun, T. Wang, H. J. Gao, Observer-based fuzzy adaptive event-triggered control for pure-feedback nonlinear systems with prescribed performance, IEEE Trans. Fuzzy Syst. 27 (11) (2019) 2152–2162.
28. L. Y. Xin, Y. G. Hong, Observer-based fuzzy adaptive event-triggered control codesign for a class of uncertain nonlinear systems, IEEE Trans. Fuzzy Syst 26 (3) (2018) 1589–1599.
29. L. Zhang, G. Yang, Observer-based fuzzy adaptive sensor fault compensation for uncertain nonlinear strict-feedback systems, IEEE Transactions on Fuzzy Systems 26 (4) (2018) 2301–2310. doi:10.1109/TFUZZ.2017.2772879.
30. L. Cao, H. Li, N. Wang, Q. Zhou, Observer-based event-triggered adaptive decentralized fuzzy control for nonlinear large-scale systems, IEEE Trans. Fuzzy Syst. 27 (6) (2019) 1201–1214.
31. C. H. Zhang, G. H. Yang, Event-triggered adaptive output feedback control for a class of uncertain nonlinear systems with actuator failures, IEEE Trans. Cybern. 50 (1) (2020) 201–210.
32. P. Tabuada, Event-triggered real-time scheduling of stabilizing control tasks, IEEE Trans. Automa. Control 52 (9) (2007) 1680–1685.
33. T. Liu, Z. P. Jiang, A small-gain approach to robust event-triggered control of nonlinear systems, IEEE Trans. Automa. Control 60 (8) (2015) 2072–2085.
34. P. Tallapragada, N. Chopra, On event triggered tracking for nonlinear systems, IEEE Trans. Au-

tom. Control 58 (9) (2013) 2343–2348.
35. E. Garcia, P. J. Antsaklis, Model-based event-triggered control for systems with quantization and time-varying network delays, IEEE Trans. Autom. Control 58 (2) (2013) 422–434.
36. A. Adaldo, F. Alderisio, D. Liuzza, G. Shi, D. V. Dimarogonas, M. di Bernardo, K. H. Johansson, Event-triggered pinning control of switching networks, IEEE Trans. Control Netw. Syst. 2 (2) (2015) 204–213.
37. A. Q. Wang, L. Liu, J. B. Qiu, G. Feng, Event-triggered robust adaptive fuzzy control for a class of nonlinear systems, IEEE Trans. Fuzzy Syst. 27 (8) (2019) 1648–1657.
38. Y. X. Huang, Y. G. Liu, Practical tracking via adaptive event-triggered feedback for uncertain nonlinear systems, IEEE Trans. Automa. Control 64 (9) (2019) 3920–3927.
39. L. T. Xing, C. Y. Wen, Z. T. Liu, H. Y. Su, J. P. Cai, Event-triggered adaptive control for a class of uncertain nonlinear systems, IEEE Trans. Automa. Control 62 (4) (2017) 2071–2076.
40. L. T. Xing, C. Y. Wen, Z. T. Liu, H. Y. Su, J. P. Cai, Event-triggered output feedback control for a class of uncertain nonlinear systems, IEEE Trans. Automa. Control 64 (1) (2019) 290–297.
41. B. Xian, M. S. D. Queiroz, D. M. Dawson, M. L. Mcintyre, A discontinuous output feedback controller and velocity observer for nonlinear mechanical systems, Automatica 40 (4) (2004) 695–700.
42. W. A. Apaza-Perez, J. A. Moreno, L. Fridman, Global sliding mode observers for some uncertain mechanical systems, IEEE Trans. Autom. Control 65 (3) (2020) 1348–1355.
43. H. Ma, H. Li, H. Liang, G. Dong, Adaptive fuzzy event-triggered control for stochastic nonlinear systems with full state constraints and actuator faults, IEEE Trans. Fuzzy Syst. 27 (11) (2019) 2242–2252.
44. C. H. Zhang, G. H. Yang, Event-triggered adaptive output feedback control for a class of uncertain nonlinear systems with actuator failures, IEEE Trans. Cybern. 50 (1) (2020) 201–210.
45. S. Haggag, D. Alstrom, S. Cetinkunt, A. Egelja, Modeling, control, and validation of an electro-hydraulic steer-by-wire system for articulated vehicle applications, IEEE/ASME Trans. Mechatronics 10 (6) (2005) 688–692.
46. Y. Yamaguchi, T. Murakami, Adaptive control for virtual steering characteristics on electric vehicle using steer-by-wire system, IEEE Trans. Ind. Electron. 56 (5) (2009) 1585–1594.
47. A. Baviskar, J. R. Wagner, D. M. Dawson, An adjustable steer-by-wire haptic-interface tracking controller for ground vehicles, IEEE Trans. Veh. Technol. 58 (2) (2009) 546–554.
48. Z. Sun, J. C. Zheng, Z. H. Man, M. Y. Fu, R. Q. Lu, Nested adaptive super-twisting sliding mode control design for a vehicle steer-by-wire system, Mech. Syst. Signal Process. 122 (2019) 658–672.
49. C. Makkar, G. Hu, W. G. Sawyer, W. E. Dixon, Lyapunov-based tracking control in the presence of uncertain nonlinear parameterizable friction, IEEE Trans. Automat.Control 52 (10) (2007) 1988–1994.
50. J. Na, Q. Chen, X. M. Ren, Y. Guo, Adaptive prescribed performance motion control of servo mechanisms with friction compensation, IEEE Trans. Ind. Electron. 61 (1) (2014) 486–494.
51. L. X. Wang, Stable adaptive fuzzy control of nonlinear systems, IEEE Trans. Fuzzy Syst 1 (22) (1993) 146–155.
52. A. Polyakov, Nonlinear feedback design for fixed-time stabilization of linear control systems, IEEE Trans. Autom. Control, 57 (8) (2012) 2106–2110.
53. Z. Zhu, Y. Xia, M. Fu, Attitude stabilization of rigid spacecraft with finite-time convergence, Int. J. Robust Nonlinear Control 21 (6) (2011) 686–702.
54. J. Yu, P. Shi, L. Zhao, Finite-time command filtered backstepping control for a class of nonlinear systems, Automatica 92 (6) (2018) 173–180.
55. S. Yu, X. Yu, B. Shirinzadeh, Z. Man, Continuous finite-time control for robotic manipulators with terminal sliding mode, Automatica 41 (11) (2005) 1957–1964.
56. H. K. Khali, Adaptive output feedback control of nonlinear systems represented by input-output models, IEEE Trans. Autom. Control 41 (2) (2013) 177–188.
57. W. Zhu, Z.-P. Jiang, Event-based leader-following consensus of multi-agent systems with input time delay, IEEE Trans. Autom. Control 60 (5) (2015) 1362–1367.

Figures

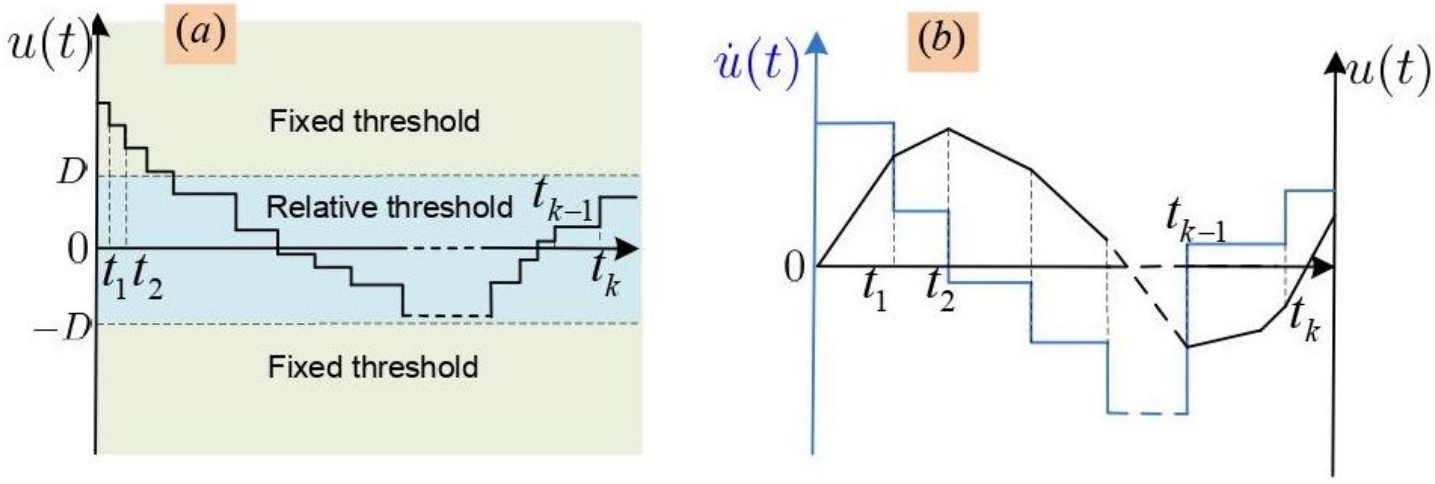

Figure 1

Please see the Manuscript PDF file for the complete figure caption

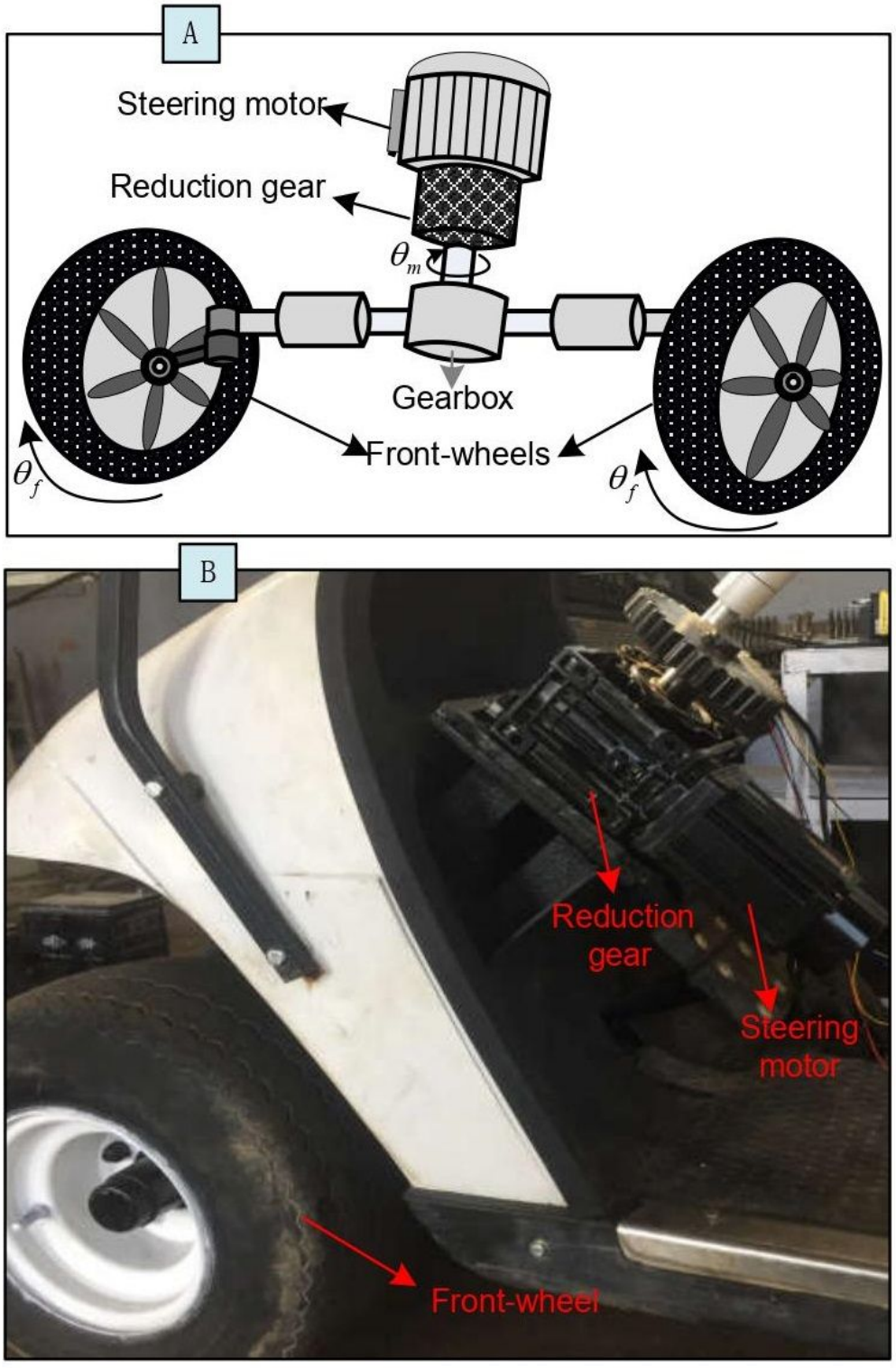

Figure 2

Please see the Manuscript PDF file for the complete figure caption

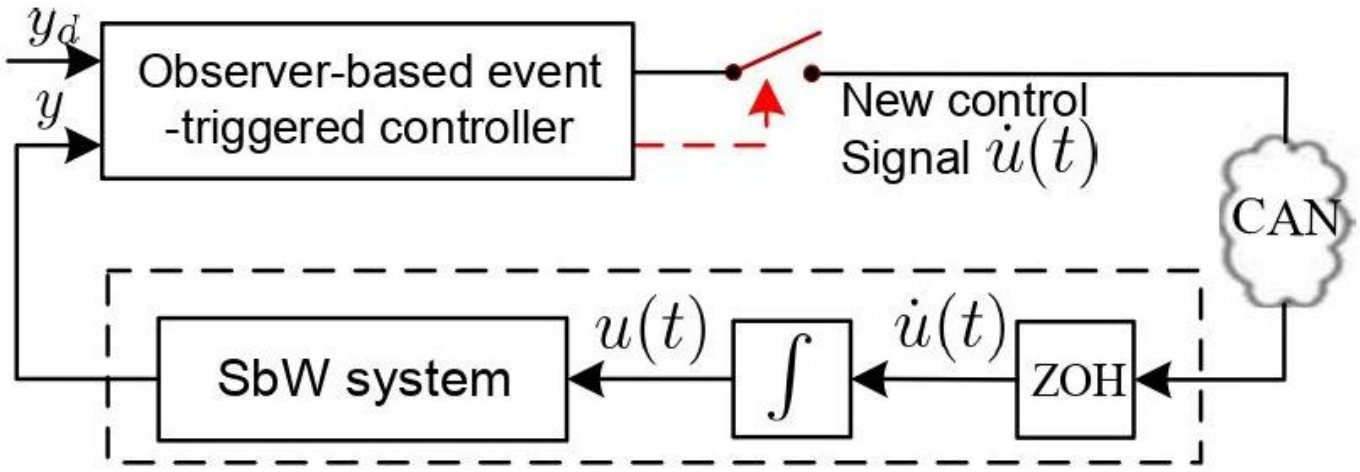

Figure 3

Please see the Manuscript PDF file for the complete figure caption

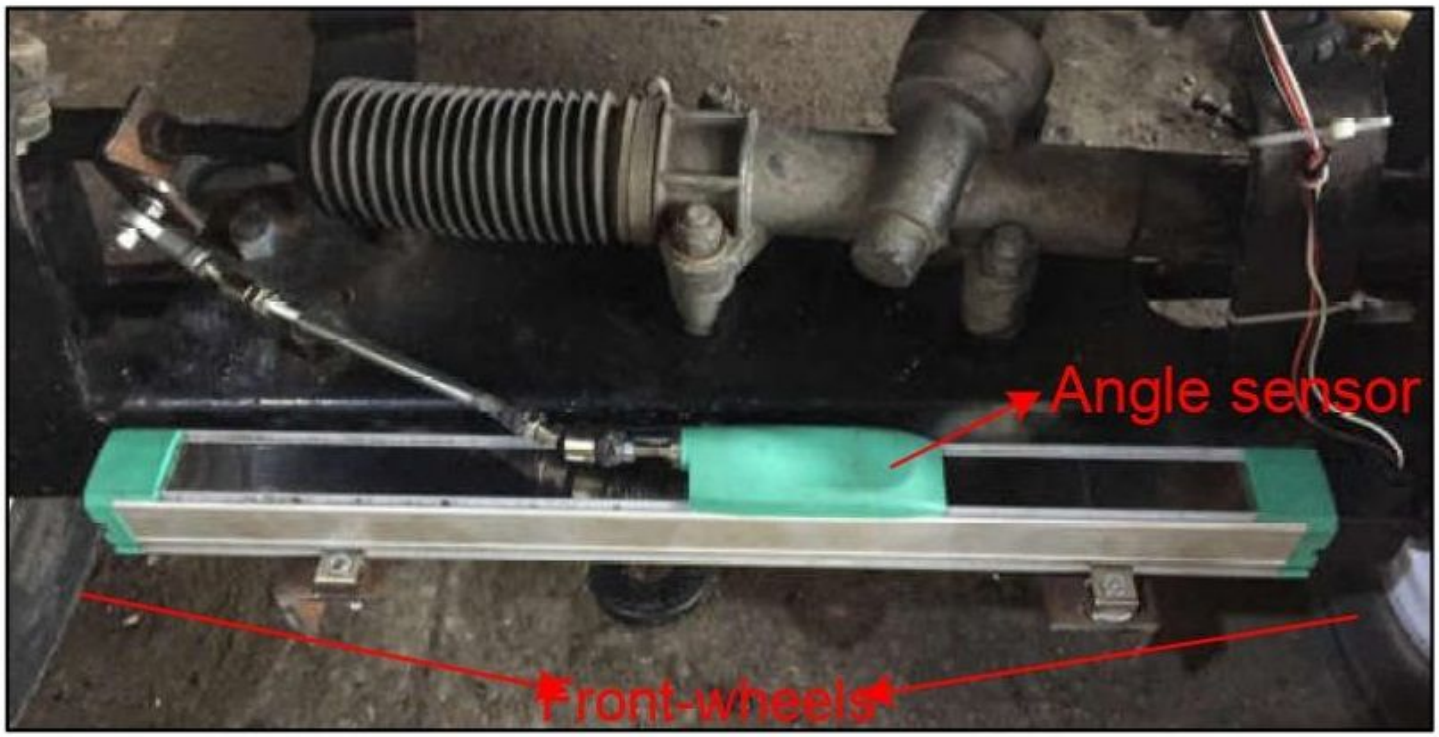

Figure 4

Please see the Manuscript PDF file for the complete figure caption

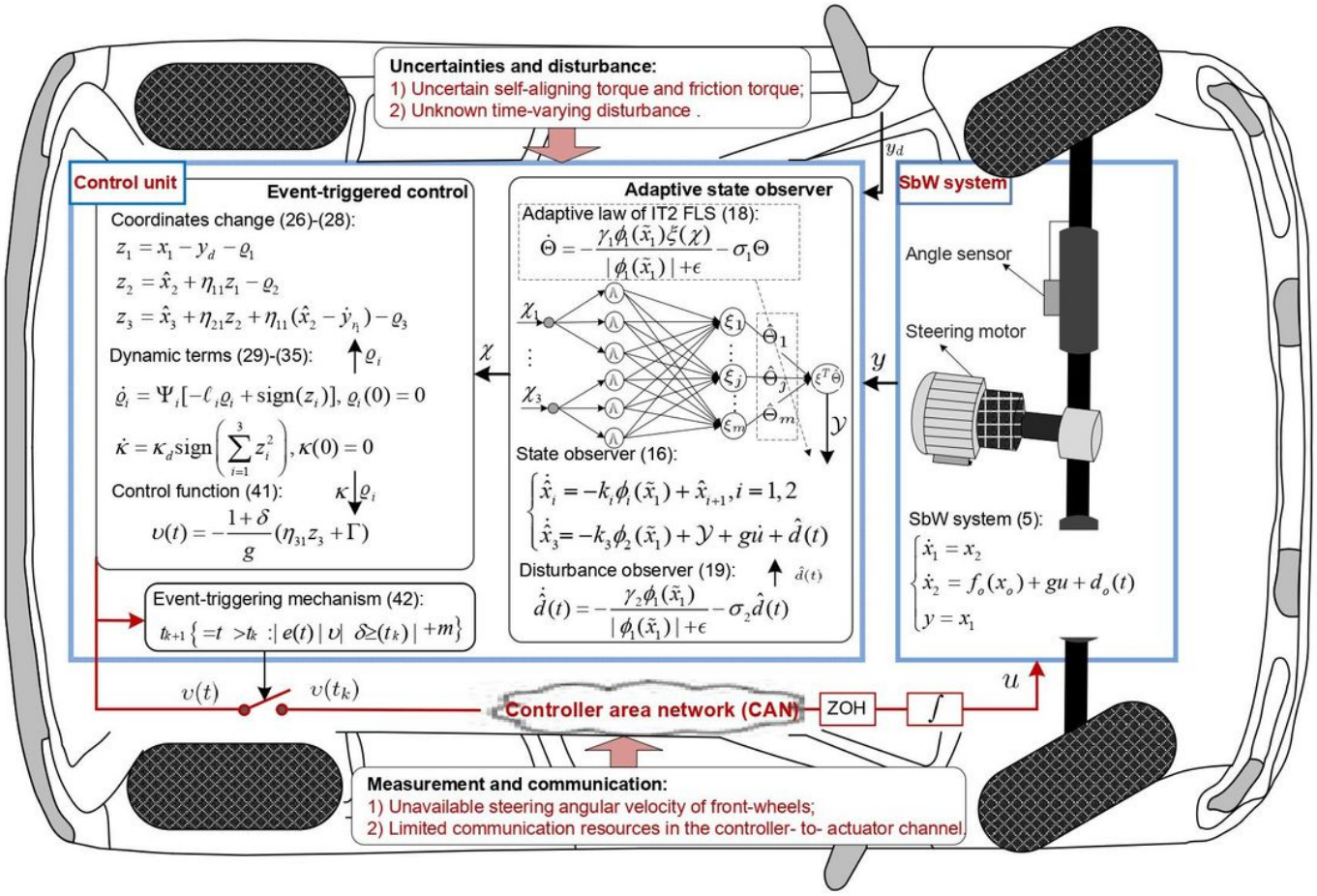

Figure 5

Please see the Manuscript PDF file for the complete figure caption

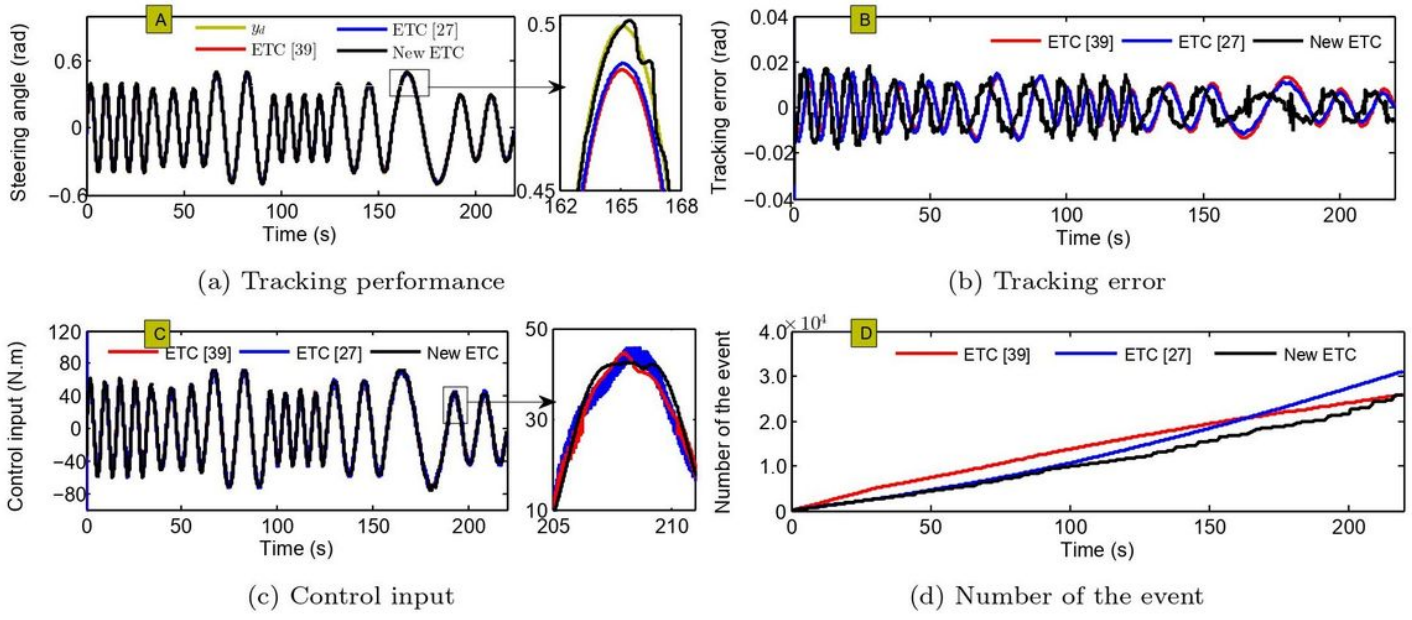

(a) Tracking performance (b) Tracking error

(c) Control input (d) Number of the event

Figure 6

Please see the Manuscript PDF file for the complete figure caption

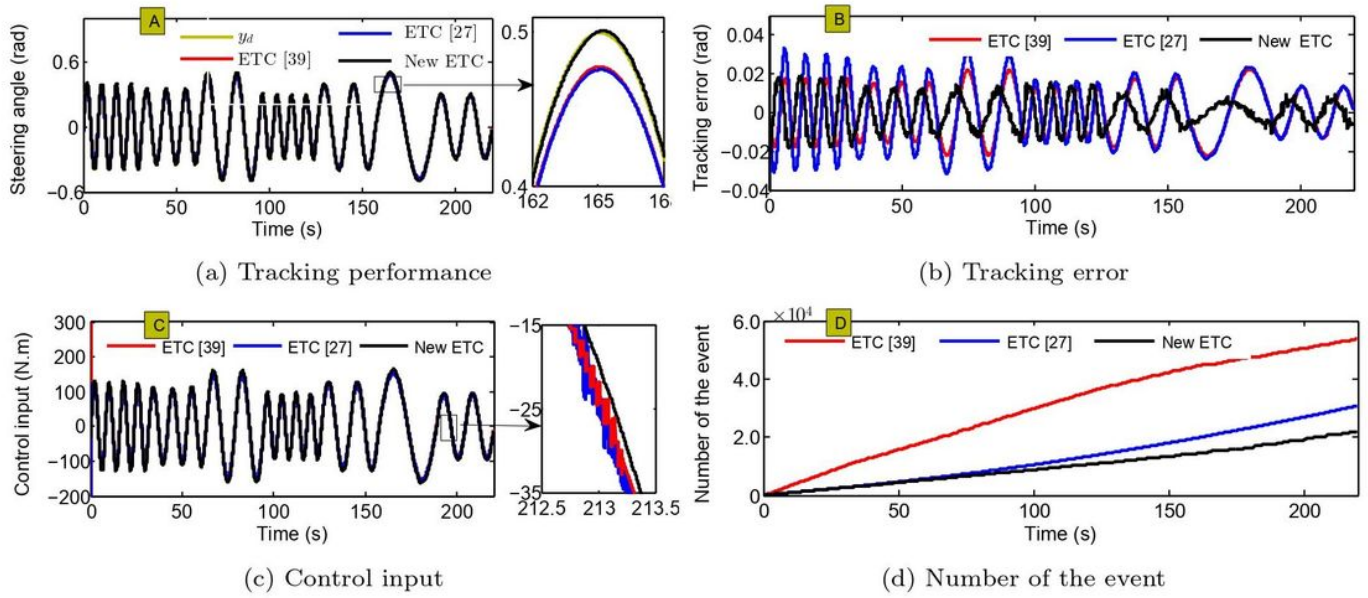

Figure 7

Please see the Manuscript PDF file for the complete figure caption

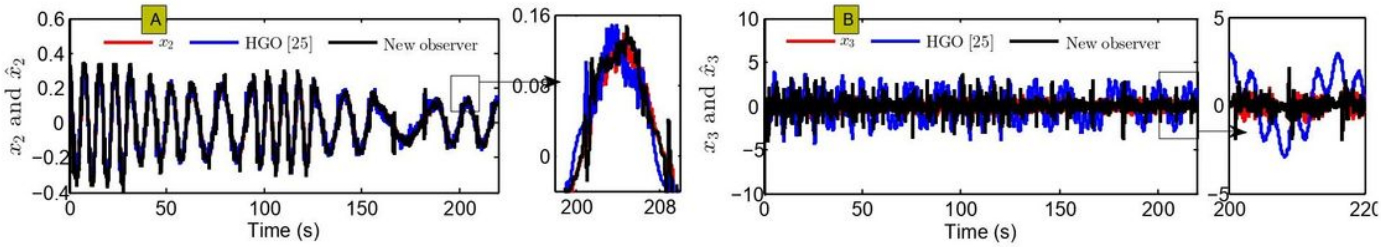

Figure 8

Please see the Manuscript PDF file for the complete figure caption

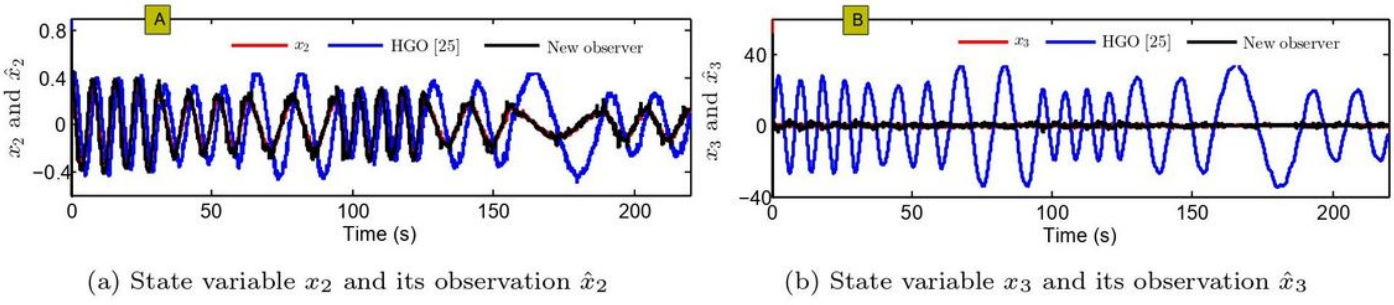

Figure 9

Please see the Manuscript PDF file for the complete figure caption

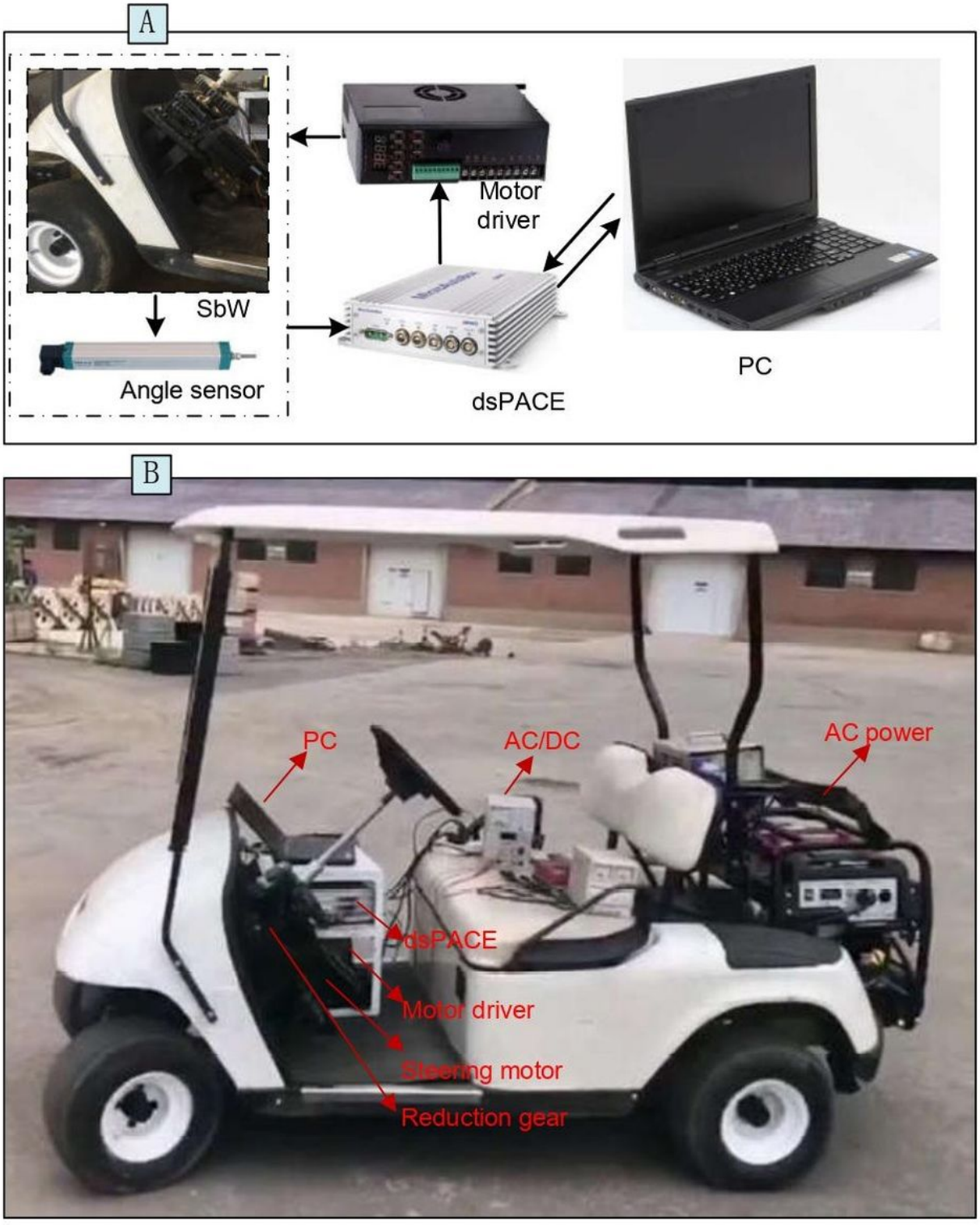

Figure 10

Please see the Manuscript PDF file for the complete figure caption

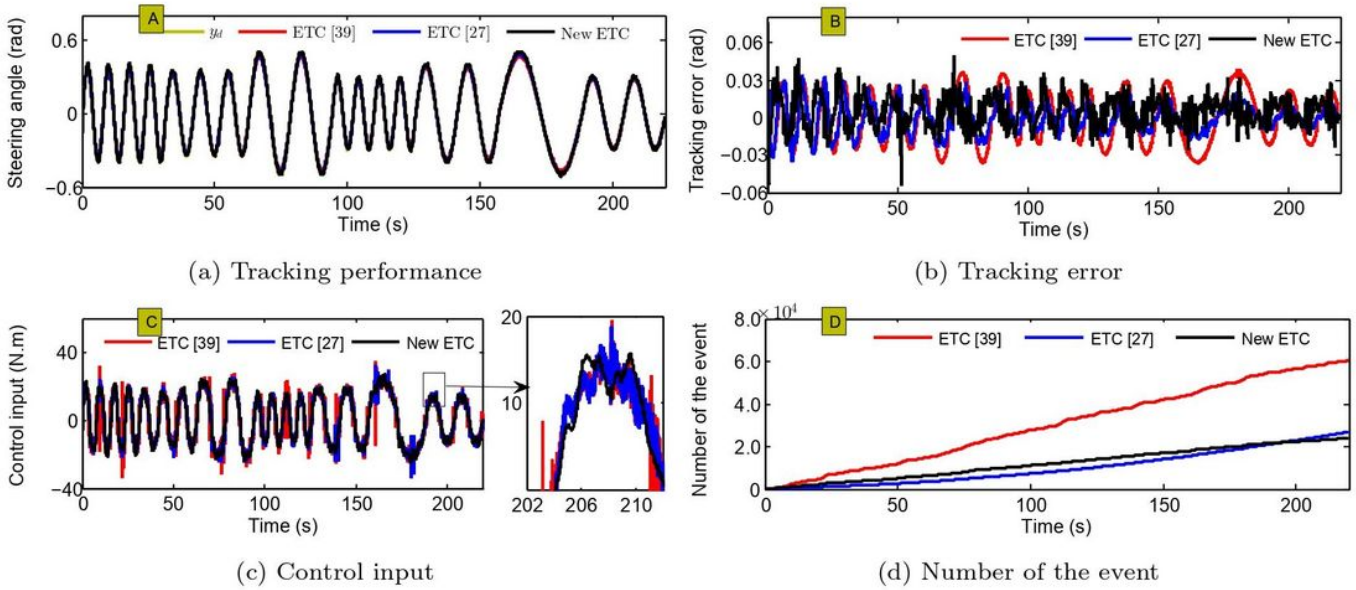

Figure 11

Please see the Manuscript PDF file for the complete figure caption

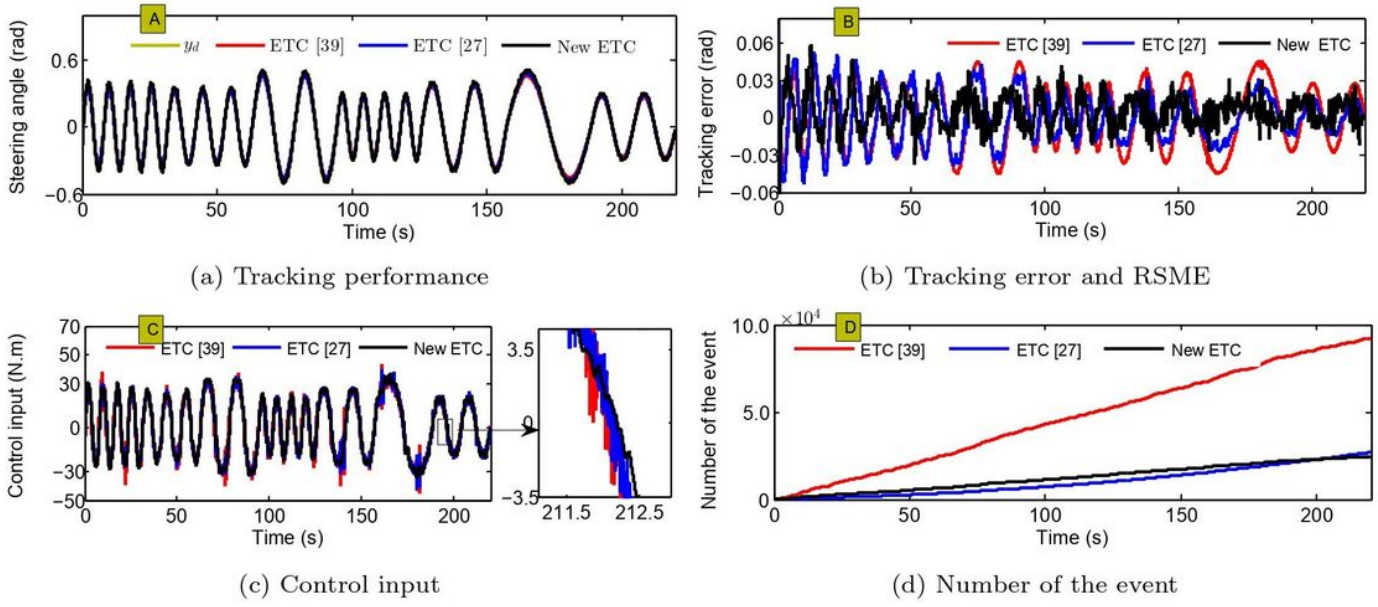

Figure 12

Please see the Manuscript PDF file for the complete figure caption

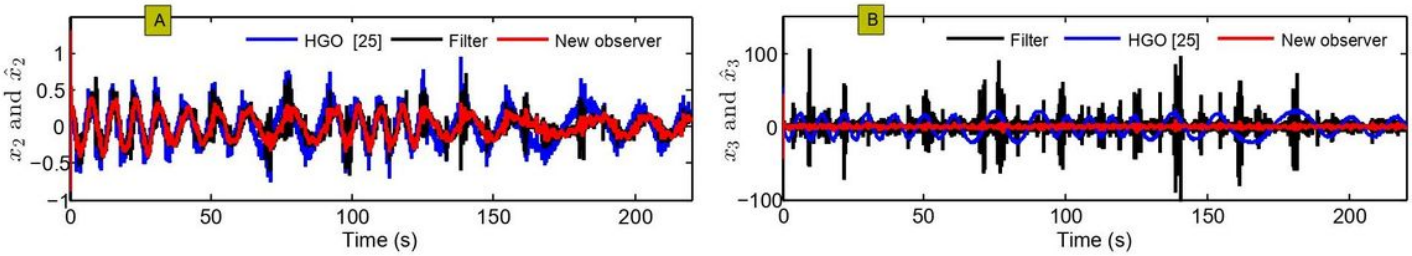

(a) State variable x_2 and its observation $\hat{x}_2$ (b) State variable x_3 and its observation $\hat{x}_3$

Figure 13

Please see the Manuscript PDF file for the complete figure caption

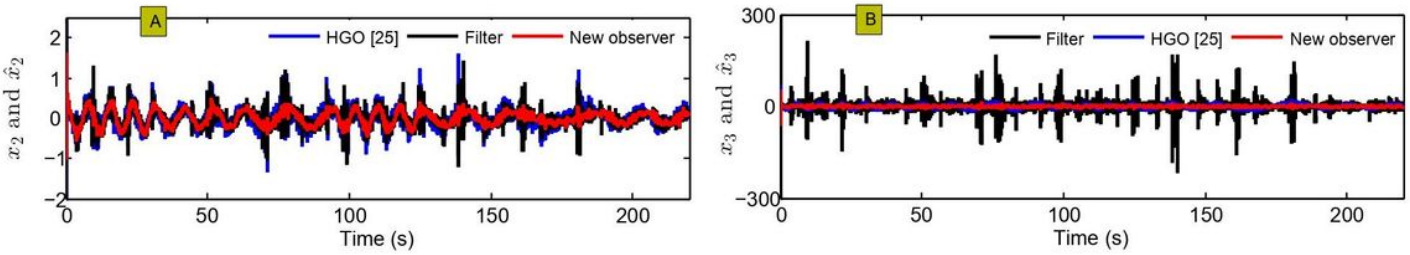

(a) State variable x_2 and its observation $\hat{x}_2$ (b) State variable x_3 and its observation $\hat{x}_3$

Figure 14

Please see the Manuscript PDF file for the complete figure caption